

1 **Bathymetric influences on Antarctic ice-shelf melt rates**

2 **D. N. Goldberg¹, T. A. Smith², S. H. K. Narayanan³, P. Heimbach^{2,4,5}, M.**
3 **Morlighem⁶**

4 ¹School of Geosciences, University of Edinburgh, Edinburgh, United Kingdom

5 ²Oden Institute for Computational Engineering and Sciences, The University of Texas at Austin, Austin,
6 Texas

7 ³Mathematics and Computer Science Division, Argonne National Laboratory

8 ⁴Jackson School of Geosciences, The University of Texas at Austin, Austin, Texas

9 ⁵Institute for Geophysics, The University of Texas at Austin, Austin, Texas

10 ⁶University of California Irvine, Department of Earth System Science, Irvine, California

Abstract

Ocean bathymetry exerts a strong control on ice sheet-ocean interactions within Antarctic ice-shelf cavities, where it can limit the access of warm, dense water at depth to the underside of floating ice shelves. However, ocean bathymetry is challenging to measure within or close to ice-shelf cavities. It remains unclear how uncertainty in existing bathymetry datasets affect simulated sub-ice shelf melt rates. Here we infer linear sensitivities of ice shelf melt rates to bathymetric shape with grid-scale detail by means of the adjoint of an ocean general circulation model. Both idealised and realistic-geometry experiments of sub-ice shelf cavities in West Antarctica reveal that bathymetry has a strong impact on melt in localised regions such as topographic obstacles to flow. Moreover, response of melt to bathymetric perturbation is found to be non-monotonic, with deepening leading to either increased or decreased melt depending on location. Our computational approach provides a comprehensive way of identifying regions where refined knowledge of bathymetry is most impactful, and also where bathymetric errors have relatively little effect on modelled ice sheet-ocean interactions.

1 Introduction

The bathymetry of the ocean exerts a leading order influence on ocean circulation, both at global and regional scales (e.g., Roberts & Wood, 1997; D. Marshall, 1995; Hughes & Killworth, 1995; Gille et al., 2004). It plays a key role in regulating exchanges between the Antarctic continental shelf and the deep ocean (e.g., Walker et al., 2013; Thoma et al., 2008; Graham et al., 2016; Thompson et al., 2018) and in setting circulation patterns on the continental shelf (e.g., Padman et al., 2010; Jacobs et al., 2011; Arneborg et al., 2012; Cochran & Bell, 2012; De Rydt et al., 2014; Rosier et al., 2018; Wählin et al., 2020). Its role in ice sheet-ocean interactions is accentuated by the fact that a large part of the Antarctic ice sheet rests well below sea level (Bentley et al., 1960), with a sizable portion of its margins terminating in large floating ice shelves. These ice shelves slow the speed of fast-flowing ice streams through buttressing (Thomas & Bentley, 1978; Thomas, 1979). Therefore the collapse or retreat, melting and associated thinning of ice shelves, while having a limited direct effect on sea level (Jenkins & Holland, 2007), can result in increased grounded ice loss from the continent (Shepherd et al., 2004) – a loss which may be amplified due to a positive feedback involving the geometry of sub-ice sheet topography known as the Marine Ice Sheet Instability (Schoof, 2007; Joughin et al., 2014).

43 The circulation of water under ice shelves is of great importance in the Amund-
44 sen and Bellingshausen Seas, West Antarctica, where intrusions of warm, salty Circum-
45 polar Deep Water (CDW) from the Antarctic Circumpolar Current occur (Jacobs et al.,
46 1996; Jenkins et al., 1997; Thoma et al., 2008; Arneborg et al., 2012; Jenkins et al., 2016;
47 Zhang et al., 2016), promoted in part by continental shelf geometry in these regions (Pritchard
48 et al., 2012). Regional atmospheric forcing and sea-ice states lead to stable stratifica-
49 tion of the water column that limits mixing of this dense water with cool surface layers
50 (Petty et al., 2013), allowing higher rates of ice-shelf mass loss than elsewhere in Antarc-
51 tica (Jenkins, 2016). CDW-driven ice-shelf melt is not strictly limited to the Amund-
52 sen and Bellingshausen Seas (Gwyther et al., 2014; Greene et al., 2017), and climate mod-
53 elling suggests it could become more widespread around Antarctica under climate change
54 scenarios (Hellmer et al., 2012). The ability of this warm, dense water to drive ice-shelf
55 melt depends to a large extent on how it is steered or blocked by bathymetry on the con-
56 tinent shelf and within the cavity.

57 Despite considerable efforts devoted to improving Antarctic-wide estimates of bed
58 topography (see most recently Morlighem et al. (2020)), our knowledge of bathymetry
59 in large parts of the marine margins of the ice sheet is highly uncertain. Direct obser-
60 vations of the ocean seafloor near Antarctica are beset by difficulties such as remoteness
61 and sea ice cover (Nitsche et al., 2007). Collecting bathymetric data under floating ice
62 shelves is even less practical. Autonomous submersibles capable of measurements un-
63 der floating ice shelves are only beginning to be deployed. With a ~ 300 m swath, they
64 provide relatively small coverage of sub-ice-shelf cavity bathymetry (e.g., Jenkins et al.,
65 2010). Airborne gravity sensing offers an alternative means of bathymetric measurement
66 (e.g., Tinto & Bell, 2011; Millan et al., 2017); however, gravimetric inversions are sub-
67 ject to errors related to resolution and geologic uncertainty. Seismic observations of the
68 bed do not rely on lithology assumptions, but as they are generally ground-based, data-
69 gathering is expensive and often limited to point estimates (e.g., Rosier et al., 2018).

70 Previous studies have addressed this uncertainty in the context of a physical ocean
71 model by considering idealised bathymetries (De Rydt et al., 2014; Zhao et al., 2018) or
72 testing different bathymetry products (Schodlok et al., 2012; Goldberg et al., 2019). To
73 date, no modelling study has investigated the melt response to the full range of uncer-
74 tainty in sub-ice shelf bathymetry. Here, we aim to provide a better understanding of

75 this uncertainty by estimating the sensitivity of ocean-driven ice-shelf melt rates to bathymetry
76 in a West Antarctic sector.

77 Previously, Losch & Heimbach (2007) developed a method to calculate the sensi-
78 tivity of circulation metrics (e.g., the strength of meridional overturning or zonal mass
79 transport) to ocean bathymetry using the adjoint of the Massachusetts Institute of Tech-
80 nology general circulation model (MITgcm). In general, adjoint models generate linearized
81 sensitivities of model outputs to an arbitrarily large set of input parameters (Wunsch,
82 1996), providing a computationally efficient means for investigating the impacts of grid-
83 scale uncertainties. To avoid tedious “by-hand” differentiation of a complex ocean gen-
84 eral circulation model, Losch & Heimbach (2007) made use of *algorithmic differentia-*
85 *tion* (AD) software, which has been used extensively with the MITgcm (Heimbach et al.,
86 2005; Wunsch et al., 2009). However, this adjoint model involving bathymetry sensitiv-
87 ities was not applied to sub-ice shelf circulation.

88 In this paper, we “revive” the adjoint model infrastructure for treating bathymetry
89 as an uncertain input variable, and employ this framework to investigate the impacts of
90 bathymetric uncertainty on ice-shelf melt rates. Two important technical improvements
91 are (i) the use of an open-source AD tool to generate the adjoint model, and (ii) improved
92 treatment of the implicit free-surface solver in generating the adjoint model. These are
93 summarized in Section 2, where we briefly discuss our methodology, including our ad-
94 joint approach and our updates to the MITgcm code base (with further details in Ap-
95 pendix A). We apply our framework to an idealised domain and analyse the resulting
96 sensitivities (Section 3). We then carry out a study of the Crosson and Dotson ice shelves
97 in the Amundsen Sea Embayment (Section 4), and conclude with discussion in Section
98 5.

99 **2 Methodology**

100 **2.1 Modelling of ice-ocean interactions**

101 We simulate sub-ice shelf circulation with the MITgcm, an open-source general pur-
102 pose finite-volume code which solves the hydrostatic primitive equations on the rotat-
103 ing sphere governing ocean flow (J. Marshall et al., 1997). (The code has nonhydrostatic
104 capability but it is not used in this study.) Since its inception, code “packages” repre-
105 senting modularized parameterizations, numerical algorithms, and separate climate com-

106 ponents have been introduced. One such package, SHELFICE (Losch, 2008), allows for
 107 circulation in cavities beneath ice shelves that may be many hundreds of meters deep.
 108 SHELFICE also calculates melt rates and the associated heat and salt fluxes at the ice-
 109 ocean interface based on under-ice ocean properties using a viscous sublayer parameter-
 110 ization (Holland & Jenkins, 1999). In this study we use the velocity-dependent form of
 111 the melt parameterization (Dansereau et al., 2014). The ice-ocean model has success-
 112 fully run the Ice Shelf Ocean Model Intercomparison Experiment (ISOMIP; Holland et
 113 al. (2003)), the experimental setup of which forms the basis for our first experiment.

114 2.2 Discretization of bathymetry in the MITgcm

115 The vertical discretization of bathymetry in MITgcm is distinct from other aspects
 116 of discretization in the model, and given the nature of this study it deserves mention.
 117 To allow for varying bathymetry but avoid dramatic steps due to the prescribed verti-
 118 cal level thicknesses, a *partial cell* discretization is implemented (Adcroft et al., 1997),
 119 where bottom cells can be partially fluid-filled with fraction h_f , down to a minimum spec-
 120 ified thickness $h_{f,min}$. This means that horizontal cell faces are partially fluid-filled as
 121 well, which is important as cell faces determine volume and tracer transport. Due to mem-
 122 ory requirements, bathymetry is represented as piecewise-constant (as opposed to piecewise-
 123 linear), meaning fluid fractions at cell faces are a function of depth at adjacent cell cen-
 124 ters (see Fig. 1(a)). This choice has implications for algorithmic differentiation of bot-
 125 tom sensitivity, as discussed below.

126 2.3 Adjoint model

127 An ocean model may be conceptualised as a mathematical function that maps an
 128 input vector \mathbf{x}_{in} onto an output vector \mathbf{x}_{out} . The input vector \mathbf{x}_{in} consists of the dis-
 129 cretized initial conditions for the oceanic state, as well as all inputs required to integrate
 130 the partial differential equations that govern the circulation of the ocean, including dis-
 131 cretized input fields for surface (forcing) and bottom (bathymetry) boundary conditions.
 132 \mathbf{x}_{out} consists of all prognostic model output (generally of a much higher dimension than
 133 that of \mathbf{x}_{in}), or diagnostic functions thereof, including scalar-valued metrics. It is often
 134 of interest to know how perturbations in \mathbf{x}_{in} affect \mathbf{x}_{out} , or how they affect quantities
 135 that depend on \mathbf{x}_{out} (sometimes referred to as "objective functions" or "quantities of in-
 136 terest"). An example application of an adjoint model might be investigating how Atlantic

137 meridional overturning is sensitive to global patterns of precipitation (Pillar et al., 2016;
138 Smith & Heimbach, 2019).

139 The *sensitivity vector*, i.e. the gradient of the quantity of interest with respect to
140 \mathbf{x}_{in} , could be determined by perturbing separately each element of \mathbf{x}_{in} and observing
141 the model response (formally, inferring a directional derivative); however, such an ap-
142 proach for computationally intensive models and input vectors of high dimension is im-
143 practical. However, forming the *adjoint* of the model (or, more precisely, the adjoint of
144 its Jacobian) provides an alternative (Errico, 1997), enabling calculation of the sensitiv-
145 ity vector at a computational cost that does not depend on the dimension of \mathbf{x}_{in} .

146 Differentiation of the ocean model can be carried out at the equation level (Sirkes
147 & Tziperman, 1997), though this approach requires a separate code that must be up-
148 dated when the ocean model is modified. Another method – and the one used in this work
149 – is Algorithmic Differentiation (AD), which uses a software tool to automate differen-
150 tiation of the model at the discrete (code) level. In this study, two different AD tools are
151 used: *Transformations of Algorithms in Fortran* (TAF; Giering et al. (2005)) and Ope-
152 nAD (Utke et al., 2008). Both are source-to-source tools, meaning code is generated in
153 the native language (as opposed to operator-overloading). Both tools have been used to
154 generate the MITgcm adjoint; TAF, a commercial product, has been used more exten-
155 sively with the MITgcm, while OpenAD is a more recent open-source tool.

156 While AD presents great benefits in differentiating complex numerical codes and
157 keeping the adjoint code in synchronization with the parent numerical code, some de-
158 gree of manual intervention is generally required. In the present study changes to the
159 adjoint generation were necessary to facilitate efficient computation, the foremost deal-
160 ing with the way in which MITgcm evolves the ocean free surface. These and other de-
161 tails as discussed in detail in Appendix A.

162 **3 Idealised Experiment**

163 To gain insight into how bathymetry modulates the interaction between ocean cir-
164 culation and ice shelf melt, we first examine sensitivity of melt to bathymetry in an ide-
165 alized domain, which is a slightly modified version of the computational domain used in
166 the Ice Shelf Ocean Model Intercomparison Project (ISOMIP; Holland et al. (2003)). In
167 the MITgcm implementation of the standard ISOMIP setup, the ocean circulates within

168 a closed rectangular domain with a flat bathymetry of 900 m depth. A zonally-uniform
 169 ice-shelf draft slopes meridionally from 700 m depth to 200 m depth over about 450 km,
 170 and is constant north of this point. We use a resolution of 30 m in the vertical, 0.3° zon-
 171 ally, and 0.1° meridionally. A full description can be found in Losch (2008). We mod-
 172 ify the ISOMIP domain by introducing a zonally-constant ridge in the bathymetry just
 173 south of the point of deepening of the ice shelf. The meridional expression is a half-cosine
 174 “bump” with a width of 2° latitude and a height of 200 m above the uniform seafloor
 175 (Fig. 2(a)), and we refer to our experiment as “ISOMIP-bump”. This bathymetry is in-
 176 spired by bathymetric ridges identified under a number of Antarctic ice shelves (e.g., Jenk-
 177 ins et al., 2010; Wei et al., 2019), which are found to strongly control the transport of
 178 relatively warm water within ice shelf cavities (De Rydt et al., 2014; Dutrieux et al., 2014).

179 Our adjoint experiment is as follows: the ISOMIP-bump model is run forward in
 180 time for 2 model years, and the spatial integral of the melt rate in the final time step
 181 is evaluated as our quantity of interest J :

$$182 \quad J = \sum_i d_i m_i, \quad (1)$$

183 where d_i and m_i are the area of, and melt rate within, horizontal cell i . The adjoint model
 184 accumulates sensitivity of J with respect to bathymetry back in time along the 2-year
 185 simulation trajectory and thus depends on the state of the entire 2-year run, not just the
 186 final state. Thus, to mitigate impacts of equilibration, we begin the model run from a
 187 “spun-up” state rather than a quiescent one. The model is thus first spun-up for 3 years,
 188 and the resulting state forms the initial conditions for our 2-year forward and adjoint
 189 run.

190 The melt rate at the final time in the adjoint experiment (Fig. 2(b)) is broadly sim-
 191 ilar with that of Mathiot et al. (2017) (their Fig. 2), although our peak melt rate is larger,
 192 and there is a “tongue” of melt rates bisecting the accretion region over the ridge. The
 193 barotropic circulation also differs slightly with respect to the standard ISOMIP exper-
 194 iment: rather than a broad cyclonic gyre, there is a narrow anticyclonic anomaly on the
 195 north side of the ridge (Fig. 2(b)). Barotropic flow is primarily along the ridge, cross-
 196 ing it primarily near the eastern and western boundaries, similar to what has been shown
 197 in a simplified two layer model (Zhao et al., 2018). Zonally-averaged temperatures (Fig.
 198 2(a)) suggest slightly cooler waters at depth just south of the ridge as opposed to the
 199 northern flank. The slightly larger melt rates as compared to Mathiot et al. (2017) could

200 reflect the fact that our simulation has not yet reached steady-state – indicating that the
 201 presence of the ridge increases the time to reach a new steady-state.

202 The adjoint-derived sensitivities are shown in Fig. 3(a). Positive values indicate
 203 locations where raising the seafloor will increase integrated melt, and negative values in-
 204 dicate where lowering the seafloor will increase melt. There are distinct broad-scale pat-
 205 terns in the sensitivities, particularly over the ridge itself. Across much of the zonal ex-
 206 tent of the ridge there is negative sensitivity, indicating a lowering of the ridge would in-
 207 crease melt. Near the eastern boundary, however, there is a region with strongly pos-
 208 itive sensitivities. Northward of the ridge where both bathymetry and ice draft are con-
 209 stant, there is a broad dipole pattern, with positive sensitivities toward the center and
 210 negative toward the east. In our investigation below we focus on these four regions (la-
 211 belled in Fig. 3(a)); foregoing close analysis of regions with negligible influence on melt
 212 (such as southward of the ridge), and regions where there is strong spatial variability in
 213 the sensitivity, such as the western edge of the ridge.

214 In order to ensure that adjoint sensitivity patterns did not arise from issues involv-
 215 ing Algorithmic Differentiation, both AD tools (OpenAD and TAF) were used to gen-
 216 erate sensitivities. (A similar approach was taken in in Heimbach et al. (2011).) The dif-
 217 ferences in the sensitivities, likely arising from numerical truncation, were negligible, and
 218 are not shown.

219 **3.1 Finite-amplitude perturbations of bathymetry**

220 As with any adjoint-based study, it is important to verify the adjoint-derived sen-
 221 sitivities by perturbing the input, or *control*, field in the forward model, i.e. by estimat-
 222 ing finite-difference approximations to the gradients that the adjoint model calculates.
 223 In the MITgcm this type of “gradient check” is more challenging when dealing with model
 224 bathymetry than with other control variables, as demonstrated in Fig. 1(b): finite per-
 225 turbations of bathymetry can change grid structure, for example by adding new cells to,
 226 or removing cells from, the domain. Neither operation is differentiable, and hence lin-
 227 earized sensitivities may not reflect model responses to perturbed bathymetry. Addition-
 228 ally, bathymetric perturbations may not be as anticipated, as thicknesses of cells will be
 229 adjusted by the model initialization to ensure no partial cell is thinner than $h_{f,min}$.

230 These challenges aside, we implement finite perturbations to bathymetry in order
 231 to test the results from the adjoint model, but our experiment design is intended to min-
 232 imize the above complications. Rather than perturb values in individual cells, we apply
 233 perturbation *patterns*. We carry out experiments with four separate perturbation pat-
 234 terns, naturally selected in regions of high sensitivity, where bathymetric perturbations
 235 exhibit the greatest control on melt-rates, as shown in Fig. 3. The patterns have a Gaus-
 236 sian profile:

$$237 \quad \delta R(\phi, \lambda) = \delta R_0 \exp \left(-\frac{(\phi - \phi_0)^2}{L_\phi^2} - \frac{(\lambda - \lambda_0)^2}{L_\lambda^2} \right) \quad (2)$$

238 where ϕ and λ are latitude and longitude. ϕ_0 , λ_0 , L_ϕ and L_λ vary with experiment but
 239 the location and radii of the perturbations can be seen from Fig. 4 for each region. Dif-
 240 ferent values of δR_0 are considered as described below.

241 For a given depth perturbation δR , the linear response to J predicted by the ad-
 242 joint is

$$243 \quad \delta J = \sum_i \delta J_i = \sum_i (\delta R_i) (\delta^* R_i), \quad (3)$$

244 where δR_i is the finite perturbation to bathymetry in ocean column i and $\delta^* R_i = \frac{\partial J}{\partial R_i}$
 245 is the bathymetric sensitivity in i as calculated by the adjoint. If the adjoint model is
 246 accurate, Eqn. (3) should be fairly accurate for small values of δR_i . This is the case for
 247 $\delta R_0 = 0.1$ m (Fig. 3(b)). Positive and negative perturbations are considered in regions
 248 1 and 2; in regions 3 and 4 only positive perturbations are examined as negative pertur-
 249 bations would lower bathymetry beyond the extent of the computational grid. For larger
 250 perturbations ($\delta R_0 = 10$ m), linear sensitivities give fairly accurate predictions in re-
 251 gions 2, 3 and 4; in region 1 (the center of the ridge), the linear approximation under-
 252 estimates the response. Closer inspection reveals that, when bathymetry is perturbed
 253 in the center of the ridge, a number of fluid-containing cells become empty. Similarly,
 254 when regions 1 and 2 are negatively perturbed with $\delta R_0 = 10$ m, an even larger num-
 255 ber of previously empty cells become fluid-filled. These non-differentiable changes could
 256 explain the underestimates.

257 These perturbation experiments provide insight into the mechanisms that cause
 258 the sensitivity patterns produced by the adjoint model. In these experiments, bathymet-
 259 ric perturbations cause circulation changes that are evident in the perturbed barotropic
 260 stream function field, shown in Fig. 4. A bathymetric rise in region 3 induces an anti-
 261 cyclonic region just to the west of the rise and a broad cyclonic region to the east (Fig.

262 4(c)). A rise in region 4 induces a similar pattern but with the relative sizes and strengths
263 of the cyclonic and anticyclonic regions reversed, in part due to zonal boundary constraints
264 (Fig. 4(d)). The pattern is reminiscent of the interaction between a jet and a topographic
265 rise (Huppert & Bryan, 1976; Holland et al., 2003), with the broad cyclonic cell in this
266 region (Fig. 2(b)) generating the background flow. As this cell transports water away
267 from the cold outflow from the cavity before it circulates back toward the ridge, it is likely
268 that perturbations which strengthen/oppose this circulation will increase/decrease melt,
269 explaining the sensitivity pattern north of the ridge.

270 On the ridge itself, there is a similar response to bathymetric bumps in regions 1
271 and 2 (Fig. 4(a,b)), although complicated by the varying background topography. In the
272 case of a raised bump on the eastern ridge, the leading effect on the circulation is a south-
273 ward shift of the warm jet travelling eastward along the ridge, increasing warm-water
274 transport into the cavity, and increasing melt. A depression in the center of the ridge
275 has a similar effect.

276 While these results are highly idealized, they are nonetheless instructive regard-
277 ing bathymetric influence on melt in ice-shelf cavities with topographic obstacles: (1)
278 bathymetry in areas “protected” by the obstacle play a relatively small role in control-
279 ling melt; (2) the height of the obstacle has a strong influence on melt, but the direc-
280 tion, or sign, of the influence may depend on the location along the ridge and related to
281 the background flow that is set up by the geometry; and (3) bathymetry oceanward of
282 the obstacle can influence melt as well, by controlling the circulation that brings warm
283 water toward the ice-shelf cavity. These insights inform the interpretation of sensitiv-
284 ities in simulations with realistic bathymetry.

285 **4 Realistic experiment: Dotson and Crosson ice shelves**

286 The Dotson and Crosson Ice Shelves are relatively small but strongly thermally-
287 forced ice shelves in the Amundsen Sea Embayment of West Antarctica (Fig. 5(a)). Re-
288 cently, these ice shelves, as well as the ice streams that flow into them, have been the
289 subject of focused glaciological and oceanographic study (e.g., Randall-Goodwin et al.,
290 2015; Goldberg et al., 2015; Miles et al., 2016; Gourmelen et al., 2017; Jenkins et al., 2018;
291 Lilien et al., 2018). Moreover, ice-ocean interactions under these ice shelves have signif-
292 icance for biological productivity in the Southern Ocean: levels of carbon sequestration

293 in the highly productive Amundsen Polynya are thought to be connected strongly to ice-
294 shelf melt volume (Gerringa et al., 2012; Yager et al., 2012). A recent modelling study
295 by Goldberg et al. (2019) showed that the choice of bathymetric product has a signif-
296 icant influence on the melt rates modelled for these ice shelves. Therefore, it is an ideal
297 region in which to examine the sensitivity of melt to bathymetry.

298 **4.1 Model configuration**

299 Our ocean model configuration is based on that of Goldberg et al. (2019). We use
300 the MITgcm with the SHELFICE package and with ice-shelf draft and bathymetry based
301 on Millan et al. (2017). At ocean-facing boundaries we impose conditions on tempera-
302 ture, salinity and velocity from a regional simulation by Kimura et al. (2017). However,
303 there are important differences with the configuration of Goldberg et al. (2019), which
304 are largely influenced by practical considerations concerning the performance of the OpenAD-
305 generated adjoint. Adjoint models generally require more computing time than the for-
306 ward models from which they derive, requiring in some cases recomputation to avoid in-
307 tractable memory requirements (Griewank & Walther, 2008). The 4-year simulations con-
308 ducted by Goldberg et al. (2019) ran for approximately 32 hours on 48 cores on the Re-
309 search Councils UK (RCUK) ARCHER supercomputer (discounting queueing times in
310 between batches), meaning an adjoint experiment might require up to several weeks' wall-
311 clock execution time leading to large delays in our investigations and potentially irre-
312 sponsible energy usage. (This scaling is based on the timings of experiments in this study
313 and not a rigorous analysis of OpenAD performance.) Thus, modifications were made
314 to reduce computational expense and facilitate adjoint computation.

315 A 2-km grid was used as opposed to a 1-km grid, and the time step increased from
316 150 to 300 seconds. Additionally, a larger horizontal eddy viscosity, $\nu_H = 300 \text{ m}^2\text{s}^{-1}$,
317 was imposed, for the following reason. The ocean adjoint model is a distinct numerical
318 code – related to the forward ocean model but with its own stability constraints, aris-
319 ing in part from the chosen quantity of interest, which informs the boundary and ini-
320 tial conditions of the adjoint model. It is often the case that the adjoint of a nonlinear
321 forward model produces sensitivity patterns with sharp spatial gradients, which grow in
322 amplitude over time because the model lacks the nonlinear feedbacks to damp them, re-
323 sulting in numerical instabilities. Hoteit et al. (2005) showed that a stabilization of the
324 adjoint may be achieved with a larger value of ν_h for the adjoint model, while retain-

325 ing a smaller eddy viscosity in the forward model, but such a capability for the OpenAD-
326 MITgcm adjoint is not yet available. We point out that our chosen value for ν_h is com-
327 parable to the ice-ocean interaction study of Dansereau et al. (2014), which also used
328 the SHELFICE package of MITgcm.

329 Additionally the open boundary conditions of our computational domain, which
330 represent interactions with the Antarctic Circumpolar Current (i.e. the ocean-facing bound-
331 ary conditions), were made time-constant rather than time-varying as in Goldberg et al.
332 (2019). As discussed in Section 4.3, this better enables the assessment of the timescale
333 of adjustment to boundary conditions. Velocity, temperature and salt conditions from
334 Kimura et al. (2017) were averaged over 2011, allowing for a shorter experiment.

335 Finally, the Millan et al. (2017) bathymetry was adjusted over a region of approx-
336 imately 90 km² close to the junction between Crosson and Dotson Ice Shelves, where the
337 Kohler range extends into the ice-shelf cavity (Fig. 5(a)). In this area, the Millan bathymetry
338 suggests a significant ridge with a peak less than 300 m below sea level. Without mod-
339 ification, this ridge would lead to very thin ocean columns in our model, effectively lim-
340 iting ocean transport to the narrow region between the ridge and Bear Peninsula. How-
341 ever, observed melt rate patterns Gourmelen et al. (2017); Goldberg et al. (2019) show
342 high melt rates in this location, suggesting a more extensive connection between the ice
343 shelves than the bathymetry product would allow. Furthermore, recent glider and float
344 observations in this region show that this ridge may be lower than suggested by the gravime-
345 try (Dutrieux et al., 2020). Our modification of this bathymetry in this region allows a
346 wider area for ocean flow while still maintaining a ridge at the Dotson-Crosson junction.
347 While our modification is not observationally grounded, our adjoint computation (de-
348 scribed below) gives an indication of the impact of this modification. If circulation in
349 this region were negligible, such assessment might not be possible.

350 Our adjoint experiment largely mirrors that of the ISOMIP-bump experiment. The
351 Dotson-Crosson model is run for 1 model year, and then the sensitivity of the objective
352 function J – the spatial integral of melt – with respect to bathymetry is computed. As
353 in our idealized experiment, we begin with a spun-up state of the model, which is steady
354 due to time-invariant forcing. The realistic experiment was carried out only with the OpenAD-
355 generated adjoint model. Even with the adjustments discussed above, the required sim-
356 ulation run-time was still well over the limits for a single job on the available HPC re-

357 sources. Therefore, further modifications were required to enable OpenAD to restart the
358 adjoint simulation over subsequent jobs. These technical modifications are referred to
359 as resilient adjoints and are described in Appendix B.

360 4.2 Results

361 Relevant aspects of the forward model are depicted in Fig. 5. Despite the lower res-
362 olution and higher viscosity compared to the configuration used by Goldberg et al. (2019),
363 the melt rate patterns are similar. Broadly consistent with observation-based inferences
364 (Randall-Goodwin et al., 2015), there is a strong outflow at the western margin of Dot-
365 son Ice Shelf – though in our model outflow is less confined to the margin, potentially
366 due to high viscosities or horizontal resolution. The total melt rate is approximately 81.5
367 Gt/yr (Fig. 7), similar to that found by Randall-Goodwin et al. (2015) for Dotson ice
368 shelf alone in January 2011. Meltrates in the simulation domain are insensitive to bathymetry
369 under much of the Dotson Ice Shelf (Fig. 6), with the exception of the connection with
370 Crosson Ice Shelf and over the small ridge at the entrance of the ice shelf (Fig. 5(a)).

371 The sensitivity pattern over the outer ridge bears similarities to the idealized ISOMIP-
372 bump experiment – with negative sensitivities in the centre of the ridge, indicating a low-
373 ering would increase melt, and positive sensitivities at the margins. The most coherent
374 pattern of sensitivity oceanward of Dotson is in the eastern side of the trough entering
375 the cavity. The negative sensitivities downslope and positive sensitivities upslope imply
376 that a steepening of the trough margin would amplify the geostrophically driven flow of
377 warm water to the ice shelf, and thus increase melting. This result is corroborated by
378 recent observational and experimental work which highlights the critical role of topog-
379 raphy in steering heat to Antarctic ice shelves (Wählin et al., 2020).

380 Under Crosson Ice Shelf, there are fairly weak but extensive positive sensitivities,
381 indicating raising of the bed would increase melt, which at first seems counter-intuitive.
382 This could arise because the cavity column depth is relatively small (on average, the col-
383 umn depth under Crosson is ~ 150 m less than under Dotson), meaning a shallower col-
384 umn would bring inflowing CDW closer to the ice shelf. Oceanward of Crosson, there
385 are coherent areas of negative sensitivity, correlating with localized bathymetric highs,
386 indicating that lowering in these regions would increase melt. However, this is not a con-

387 sistent pattern, as there is a region along the front with positive sensitivities, indicat-
 388 ing that in this shallow-bedded region, raising the bed would actually increase melt rates.

389 4.3 Equilibration of adjoint sensitivities

390 Although the adjoint model represents a differentiation of all physical processes,
 391 this does not guarantee that the adjoint run should capture the dominant linear adjust-
 392 ments associated with bathymetric influence of melt. This is because these adjustments
 393 operate over an intrinsic time scale (e.g. Heimbach & Losch, 2012), and it is difficult to
 394 know *a priori* if the adjoint run encompasses this scale.

395 The nature of our adjoint run allows us to evaluate whether this adjustment is cap-
 396 tured *a posteriori*. The bathymetry field in the ocean model ultimately affects the model
 397 through the partial cell factors h_f (*cf.* Section 2.2), and related factors h_f^w and h_f^s , the
 398 fluid-filled portion of cell faces at the southern and western sides of bottom cells. This
 399 dependency among the cell factors is set in the initialization of the model. Thus, if the
 400 *adjoint sensitivity* fields corresponding to these variables are relatively steady as the ad-
 401 joint model steps backward in time, then bathymetric sensitivities are *converged*: they
 402 would not change significantly with a longer run. In physical terms, this would imply
 403 that the length of the simulation is on order of the time scale of adjustment to pertur-
 404 bations or greater.

405 Fig. 7 shows the Euclidean norm of the δ^*h_f field, the adjoint sensitivity of h_f , as
 406 the adjoint model evolves, which it does backward in time (from month 12 to 0). Sim-
 407 ilar time series are shown for adjoint fields corresponding to the h_f^w and h_f^c fields. $\delta^*h_f^w$
 408 and $\delta^*h_f^c$ norms have roughly steadied by the end of the adjoint run (month 0), while
 409 δ^*h_f is steadily growing. However, δ^*h_f only makes a small contribution to bathymet-
 410 ric sensitivity over this time period. These results suggest the immediate effect of chang-
 411 ing bathymetry is on transport, with a timescale of about a year for the present model.
 412 However, partial cell volume, which affects, among other things, the heat content at depth,
 413 might have strong impacts on melt rate over much longer time scales, not considered here.

414 We point out that our ability to evaluate adjoint equilibration in this manner is
 415 due to our use of time-invariant controls. In adjoint experiments involving time-varying
 416 controls, such as wind forcing or time-evolving boundary conditions (e.g., Heimbach &

417 Losch, 2012), the adjoint sensitivity would not be expected to asymptotically approach
 418 a “steady state” in reverse-time.

419 **4.4 Impact of bathymetry product uncertainty**

420 As demonstrated in Goldberg et al. (2019), one application of adjoint sensitivities
 421 is in estimating the impact of an alternative data product on the quantity of interest.
 422 Recently, a new bathymetric product for Antarctica became available, BedMachine (Morlighem
 423 et al., 2020), which differs from that of Millan et al. (2017). In particular, there are large
 424 differences within the ice shelf cavities, especially for Dotson (Fig. 8(a)), as the bathymetry
 425 of Millan was later updated by using the methodology described in An et al. (2019), for
 426 which the Direct Current shift in the gravity data is not assumed to be spatially uniform.

427 In a similar fashion to the idealized finite perturbation experiments in section 3.1,
 428 we use the difference between bathymetry products as a bathymetric uncertainty esti-
 429 mate and input to Eqn. (3). This formula results in an estimated 10 Gt/yr uncertainty
 430 in Dotson and Crosson melt-rates due to bathymetric error resulting purely from the dif-
 431 ferences in these two products. Of course, this estimate is only a first order approxima-
 432 tion as it assumes that this linear term dominates any higher order (i.e. nonlinear) ef-
 433 fects. From our idealized experiments, we can expect this 10 Gt/yr uncertainty may be
 434 an underestimate. Still, it is informative to examine which areas of the ice-shelf cavities
 435 actually contribute to this increase. This can be seen from Fig. 8(b), which shows

$$436 \quad \delta J_i = (\delta R_i)(\delta^* R_i) \quad (4)$$

437 i.e. the summand of Eqn. (3), for this combination of bathymetric perturbation and ad-
 438 joint sensitivity. Despite the extensive differences in bathymetry under Dotson between
 439 the products, there are only a few regions where this difference matters, which are elu-
 440 cidated by the sensitivity pattern in Fig. 6. Most prominently, the representation of the
 441 ridge near the front of Dotson, which is far less pronounced in the BedMachine product,
 442 accounts for 4.3 Gt/yr difference in melt-rates (Fig. 8(b)).

443 **4.5 Sensitivity of grounded ice loss to ocean bathymetry**

444 Understanding the impact of ocean bathymetry on sub-ice shelf melt rates is im-
 445 portant due to the impact of melting on the loss of buttressing and grounded ice volume.
 446 The experiments above focus on melt rate as a target quantity of interest, rather than

447 grounded ice volume. To comprehensively estimate sensitivity of grounded ice volume
 448 to ocean and sub-ice sheet bathymetric uncertainty would require the adjoint to a fully
 449 coupled ice sheet-ocean model, which does not presently exist.

450 Nevertheless, with our current framework we can begin to explore pathways of sen-
 451 sitivity from ocean model inputs to ice-sheet state-related quantities of interest. In math-
 452 ematical terms, we seek the total sensitivity of ice sheet volume (as our quantity of in-
 453 terest) to bathymetry, that is, $\frac{\partial V}{\partial R_i}$ where V is grounded ice volume and R is bathymetry
 454 in location i . We emphasize that this quantity is distinct from sensitivity of grounded
 455 volume to under-ice bathymetry, which directly controls ice flow and dynamic thinning
 456 (see (e.g., Goldberg et al., 2015), their Figure 7(b)); rather, the pathway of influence con-
 457 sidered here is through control on melt rates, which in turn impact ice-shelf buttress-
 458 ing. Thus, for ocean bathymetric grid points, R_i , we may write:

$$459 \quad \frac{\partial V}{\partial R_i} = \sum_k \frac{\partial V}{\partial m_k} \frac{\partial m_k}{\partial R_i}. \quad (5)$$

460 where m_k is ocean melt rate in cell k and $\frac{\partial V}{\partial m_k}$ is the ice-sheet model derivative of grounded
 461 volume with respect to melt in cell k . While calculating sensitivity of grounded ice vol-
 462 ume to melt is beyond the scope of an ocean model, an ice-sheet model framework to
 463 do this does exist (e.g., Goldberg & Heimbach, 2013). If these sensitivities can be found,
 464 then a new quantity of interest for the ocean model can be defined:

$$465 \quad J_{gv} = (\nabla_{\mathbf{m}} V)^T \mathbf{m} \equiv \sum_k \left(\frac{\partial V}{\partial m_k} \right) m_k, \quad (6)$$

466 Note that if the first term in the inner product is external to the ocean model, then the
 467 gradient of J_{gv} with respect to R_i , ocean bathymetry in location i , is equivalent to the
 468 expression on the right hand side of Eqn. (5). A different way of seeing this is that the
 469 product “projects” patterns of ice sheet volume sensitivities to melt rates onto melt rate
 470 sensitivities to ocean bottom topography.

471 In Goldberg et al. (2019), an *ice-sheet* adjoint model was used to find the sensitiv-
 472 ity of grounded volume of Smith Glacier, the glacier that feeds Dotson and Crosson Ice
 473 Shelves, to ice-shelf melt rates (Fig. 9(a)). These ice-melt sensitivities are used to con-
 474 struct the quantity of interest J_{gv} and sensitivities with respect to ocean bathymetry are
 475 found. This result is shown in Fig. 9(b). The most striking feature of this result is the
 476 similarity of the pattern to that of Fig. 6, the sensitivity of melt to bathymetry (R^2 of
 477 0.93; see also Fig. 9(c)). Comparing Eqns. (1) and (6), the quantities of interest effec-
 478 tively differ only in a weighting of melt rate by grounded ice volume sensitivities. Thus

479 the similarity in Figs. 9(b) and 6 suggests that only *total*, or spatially integrated, melt
 480 can be strongly affected by bathymetry; whereas melt rate *patterns* are controlled by other
 481 factors such as ice-shelf geometry (Goldberg et al., 2019).

482 We point out this sequence of adjoint sensitivity calculations, in which ice-sheet
 483 sensitivity is passed to an ocean model adjoint, which is in turn used to find ocean sen-
 484 sitivity, is a simplified representation of a coupled adjoint ice-ocean model. In a prop-
 485 erly coupled model, the ocean provides melt rates to the ice sheet, while the ice sheet
 486 provides ice-shelf drafts to the ocean model, with these fields being continually updated.
 487 Ideally, in a coupled adjoint model melt sensitivities would be passed to the ocean ad-
 488 joint model and ice-draft sensitivities to the ice adjoint model with the same frequency.
 489 (In our study, ice-draft sensitivities were not calculated, but our framework could be eas-
 490 ily modified to do so.) Moreover, if the ocean and ice models are not on the same grid
 491 (as is the case with our ocean model and the ice-sheet model used by Goldberg et al. (2019)),
 492 a coupled model would interpolate the melt rates to the ice-sheet grid. Strictly, the term
 493 $(\nabla_{\mathbf{m}}V)^T$ in the definition of J_{gv} should be right-multiplied by the adjoint of this inter-
 494 polation operator. This was not done in our calculation, rather the ice-sheet adjoint sen-
 495 sitivity was interpolated to the ocean grid directly. Still, our results present a useful pre-
 496 liminary assessment of the controls of ocean bathymetry on ice-sheet volume, and can
 497 potentially inform more comprehensive assessments using coupled ice sheet-ocean mod-
 498 els.

499 5 Discussion and Conclusions

500 In this study we have applied an algorithmic differentiation (AD) framework to an
 501 ocean general circulation model in order to determine the sensitivity of ice-shelf melt rates
 502 to ocean bathymetry. A similar framework of inferring bottom topography sensitivities
 503 has been applied before (Losch & Heimbach, 2007), in a coarse-resolution global-scale
 504 model. Here, we extend this computational framework to a regional domain that includes
 505 circulation in sub-ice shelf cavities in order to assess the impact of uncertainty in bathymetry,
 506 a quantity which cannot be measured under ice-shelves by ship-based methods, on melt
 507 rates. Additionally, we have made technical improvements by avoiding the differentia-
 508 tion by the AD tool of the Poisson solver for the implicit free surface and facilitating the
 509 use of the tool in high performance computing environments (Appendices A and B). We
 510 have done so using an open-source AD tool.

511 Results from both the idealized and realistic simulations show how bathymetry near
512 and underneath ice-shelves modulate melt-rates. Ocean-ward of an ice shelf, troughs lead-
513 ing to the ice front act as a guide for incoming warm ocean waters. Specifically, we show
514 that steepening the trough in front of the Dotson ice shelf would increase melting as a
515 result of increasing the geostrophic inflow. These results provide a complementary per-
516 spective to the idealized simulations, observations, and experimental results shown in
517 Wählin et al. (2020).

518 Underneath ice shelves, it is well known that ridges or sills hinder the inflow of warm,
519 dense waters into cavities (Dutrieux et al., 2014; De Rydt et al., 2014; Slater et al., 2019;
520 Zhao et al., 2018). However, the spatial details of how these obstacles impact ice shelf
521 melting are in some instances counter-intuitive. For example, the sensitivities in our ide-
522 alised ISOMIP-bump experiment identified locations where *raising* the level of a sub-
523 ice-shelf ridge led to increased melt. These results were proven to be robust in forward
524 experiments, and they were mirrored in our Dotson-Crosson regional simulation. Thus,
525 while bathymetric obstacles do play a strong role, they do not simply serve as a “dam”
526 to hold back dense warm waters; rather, an obstacle’s impact on melt must be assessed
527 in the context of the broader ocean circulation and topographic steering of that circu-
528 lation.

529 When calculating sensitivities to bathymetry, the MITgcm adjoint is subject to non-
530 differentiable operators, and may underestimate response to some perturbations (*cf.* Fig.
531 3(b)) – though more work is needed to determine under what conditions and scales the
532 predicted melt response to bathymetric perturbations is valid. Nevertheless, our ideal-
533 ized experiments suggest the adjoint is able to identify locations and regions where to-
534 pography “matters”. Losch & Heimbach (2007) reach a similar conclusion with their study.
535 They attribute this to low model resolution, though based on our idealised experiments
536 this limitation might apply to high-resolution studies as well.

537 Regardless, such experiments provide utility to observations of sub-shelf bathymetry
538 which seek to aid modelling of ice-ocean interactions. High-resolution studies of ice-shelf
539 bathymetry (for instance, through gravity analysis and seismic inversion) are possible,
540 but are very limited in scope. As our understanding of sub-shelf bathymetry evolves, our
541 adjoint-based method could be adapted to identify candidate locations where high res-
542 olution observational campaigns can be most impactful – for instance, by assessing the

543 potential information gain in important quantities of interest, as in Loose et al. (2020).
544 Additionally, patterns of spatial variability in sensitivity (such as that seen on the flank
545 of Dotson trough) could inform requirements for airborne gravity surveys (in terms of
546 aircraft speed and altitude) to ensure such variability is captured.

547 A major use of the MITgcm adjoint model is for improved assimilation of oceano-
548 graphic data (e.g., Wunsch & Heimbach, 2007; Wunsch et al., 2009). However, it is un-
549 likely that an adjoint ocean model can be used to estimate sub-ice shelf bathymetry by
550 assimilating spatial observations of melt rates, for two reasons. Firstly, as demonstrated
551 in our idealised and realistic experiments, there are extensive regions under ice shelves
552 where melt rates are not sensitive to bathymetry. Thus two very different bathymetry
553 products (such as the Millan and BedMachine datasets) could give very similar melt rates.
554 Secondly, sub-shelf circulation seems to “filter” the effects on melt rate, such that while
555 bathymetry has a strong impact on total melt, its effect on melt rate patterns may be
556 weaker – effectively limiting the information contained in spatially resolved melt patterns
557 (Gourmelen et al., 2017). It may be possible, nevertheless, to “fine tune” our knowledge
558 of bathymetry in regions that are known to strongly impact melt rates.

559 Our study was spatially limited in that only Crosson and Dotson ice shelves were
560 modelled – but it was also *temporally* limited, with time-invariant conditions represent-
561 ing far-field heat content and thermocline depths. In reality, the depth of CDW on the
562 Amundsen shelf and elsewhere in Antarctica varies both seasonally and interannually
563 (e.g., Thoma et al., 2008; Jenkins et al., 2016; Webber et al., 2017), and it is possible that
564 this variability could impact sensitivity of melt to bathymetry. Therefore, the results in
565 Section 4 should be viewed as a preliminary exploration of bathymetric sensitivity of ice-
566 shelf melt for Antarctic ice shelves. Our methodology must be applied to simulations of
567 ice-ocean interactions that are longer-term, more spatially extensive, and validated against
568 observations of ice-shelf melt (Rignot et al., 2013; Gourmelen et al., 2017; Jenkins et al.,
569 2018) in order that the impacts of ocean bathymetry, and our uncertainty of it, upon ice-
570 shelf melt can be fully evaluated. The full potential of this work may be unleashed in
571 fully coupled forward and adjoint ocean-ice sheet calculations, in which ice sheet volume
572 sensitivities to ocean bathymetric uncertainties may be more comprehensively studied.

Appendices

A Modifications to the MITgcm adjoint

The MITgcm, and in particular a configuration using the SHELFICE physics package for an Antarctic ice shelf, has been differentiated algorithmically (Heimbach & Losch, 2012), and so no additional modifications were required for applications to ice sheet-ocean interactions. However, there are technical issues in using bathymetry as a control variable. For instance, fluid fractions at grid cell faces (see Section 2.2) are based on the minimum fraction of adjacent cells, leading to potential non-differentiability. We adopt the approach of Losch & Heimbach (2007) of “smoothing” the min/max functions, but we note that this feature has not been used outside of bathymetric sensitivity studies.

Another computational challenge in treating bathymetry as a control variable lies with the implicit solve for the free surface at each time step (J. Marshall et al., 1997). The model solves the linear system $\mathbf{A}\eta = \mathbf{b}$ for η , where η is the free surface at the next time step, and \mathbf{b} is a field arising from the baroclinic step of the model. \mathbf{A} is a linear, self-adjoint operator on η and the propagation of sensitivity from η to b can be calculated analytically:

$$\delta^*\mathbf{b} = \mathbf{A}^{-1}\delta^*\eta, \quad (7)$$

where $\delta^*\eta$ is the *adjoint sensitivity* of η and likewise for \mathbf{b} . This formulation is standard in the MITgcm for adjoint based sensitivity analyses of any control variable except for fluid depth. However, the operator \mathbf{A} depends on ocean column depth, which in the present study is a control variable, and therefore the backward-propagation of sensitivities from η to \mathbf{A} must be considered as well. Losch & Heimbach (2007) dealt with this issue by allowing the AD tool to differentiate the linear solver code; however, as it is an iterative solver, this approach requires storing intermediate variables at each solver iteration during every time step of the forward model, which hinders performance and does not scale well to high dimensional problems. Losch & Heimbach (2007) recommend, but do not implement, using the approach of Giles et al. (2002), which augments Eqn. (7) with

$$\delta^*\mathbf{A} = -\delta^*\mathbf{b} \eta^T. \quad (8)$$

In this work we implement this approach, obviating the need for the AD tool to differentiate the implicit solver.

603 B Resilient Adjoints

604 Simulation of large models requires the use of high performance computing (HPC),
 605 generally with defined job time limits. The MITgcm has a restart capability allowing to
 606 circumvent these limits: the “state” of the model is periodically saved to file, and new
 607 jobs can begin from this time stamp by reading the saved state. To restart the adjoint
 608 model, simulations must save both the forward and adjoint states – a capability referred
 609 to as *resilient adjoints*. A similar capability was previously implemented with TAF as
 610 *the Divided Adjoint* (DIVA).

611 Here we provide an overview of resilient adjoints, a strategy that enhances the de-
 612 fault checkpointing scheme used by OpenAD. Checkpointing approaches store the state
 613 of the primal (forward) computation and reduce the amount of memory that is required
 614 to compute adjoints. By default, OpenAD uses binomial checkpointing for the time-stepping
 615 loop (Griewank & Walther, 2000). Consider a computation consisting of l timesteps, with
 616 c the number of checkpoints that can be stored. Figure 10 (top) illustrates binomial check-
 617 pointing for $l = 10$ and $c = 3$.

618 A two-level checkpointing approach can build upon this approach by converting
 619 the time stepping loop into a loop nest containing l_2 outer iterations and l_1 inner iter-
 620 ations where $l = l_2 \times l_1$ (Aupy et al., 2014). The inner loop uses binomial check-
 621 pointing as before; the outer loop uses periodic checkpointing. The left part of Figure 10 (bot-
 622 tom) illustrates two level checkpointing for $l_2 = 5$, $l_1 = 10$ and $c_1 = 3$. The resilient
 623 adjoints capability enhances two level checkpointing by storing to disk the adjoint state
 624 computed at the end of each outer level iteration. To restart a computation at the gran-
 625 ularity of an l_2 timestep then, only the stored l_2 state checkpoints and the last adjoint
 626 checkpoint, if any, are required.

627 Acknowledgments and Code/Data Availability.

628 D.G. was supported by NERC Standard Grants NE/M003590/1 and NE/T001607/1.
 629 D.G. and M.M. were supported jointly by NERC-NSF ITGC Grant PROPHET. T.S.
 630 and P.H. were supported in part by NSF grant #1750035 and JPL/Caltech subcontract
 631 “ECCO: Understanding Sea Level, Ice, and Earths Climate”. S.N. was supported by the
 632 U.S. Department of Energy, Office of Science, under contract DE-AC02-06CH11357. MIT-
 633 gcm code can be accessed publicly at mitgcm.org and OpenAD from <https://www.mcs.anl.gov/OpenAD>.

634 BedMachine data is available from <https://nsidc.org/data/nsidc-0756> . Output availabil-
 635 ity information for Kimura et al. (2017) is given in their publication. All model output
 636 used to produce figures for this manuscript is provided as supporting information.

637 References

- 638 Adcroft, A., Hill, C., & Marshall, J. (1997). Representation of topography by shaved
 639 cells in a height coordinate ocean model. *Monthly Weather Review*, *125*(9), 2293-
 640 2315. Retrieved from [https://doi.org/10.1175/1520-0493\(1997\)125<2293:
 641 ROTBSG>2.0.CO;2](https://doi.org/10.1175/1520-0493(1997)125<2293:ROTBSG>2.0.CO;2) doi: 10.1175/1520-0493(1997)125(2293:ROTBSG)2.0.CO;2
- 642 An, L., Rignot, E., Millan, R., Tinto, K., & Willis, J. (2019). Bathymetry of North-
 643 west Greenland Using “Ocean Melting Greenland” (OMG) High-Resolution
 644 Airborne Gravity and Other Data. *Remote Sens.*, *11*(2). Retrieved from
 645 <https://www.mdpi.com/2072-4292/11/2/131> doi: 10.3390/rs11020131
- 646 Arneborg, L., Wählin, A. K., Björk, G., Liljebldh, B., & Orsi, A. H. (2012,
 647 Nov 25). Persistent inflow of warm water onto the central amundsen shelf. *Nature*
 648 *Geoscience*, *5*, 876–880. doi: 10.1038/ngeo1644
- 649 Aupy, G., Herrmann, J., Hovland, P., & Robert, Y. (2014, 04). Optimal multi-
 650 stage algorithm for adjoint computation. *SIAM Journal on Scientific Computing*,
 651 *38*. doi: 10.1137/15M1019222
- 652 Bentley, C. R., Crary, A. P., Ostenso, N. A., & Thiel, E. C. (1960, January). Struc-
 653 ture of West Antarctica. *Science*, *131*(3394), 131–136.
- 654 Cochran, J. R., & Bell, R. E. (2012). Inversion of icebridge gravity data for con-
 655 tinental shelf bathymetry beneath the larsen ice shelf, antarctica. *Journal of*
 656 *Glaciology*, *58*(209), 540–552. doi: 10.3189/2012JoG11J033
- 657 Dansereau, V., Heimbach, P., & Losch, M. (2014). Simulation of subice shelf melt
 658 rates in a general circulation model: Velocity-dependent transfer and the role of
 659 friction. *Journal of Geophysical Research: Oceans*, *119*(3), 1765–1790. Retrieved
 660 from <http://dx.doi.org/10.1002/2013JC008846> doi: 10.1002/2013JC008846
- 661 De Rydt, J., Holland, P. R., Dutrieux, P., & Jenkins, A. (2014). Geometric
 662 and oceanographic controls on melting beneath pine island glacier. *Journal of*
 663 *Geophysical Research: Oceans*, *119*(4), 2420–2438. Retrieved from [http://
 664 dx.doi.org/10.1002/2013JC009513](http://dx.doi.org/10.1002/2013JC009513) doi: 10.1002/2013JC009513
- 665 Dutrieux, P., De Rydt, J., Jenkins, A., Holland, P., Ha, H., Lee, S., . . . Schröder, M.

- 666 (2014). Strong sensitivity of pine island ice-shelf melting to climatic variability.
 667 Science, **343**(6167), 174–178. Retrieved from [http://science.sciencemag.org/
 668 content/343/6167/174](http://science.sciencemag.org/content/343/6167/174) doi: 10.1126/science.1244341
- 669 Dutrieux, P., Lee, C., Rainville, L., Gobat, J., Girton, J., Christianson, K., ... Mil-
 670 lan, R. (2020, February). Seaglider and Float Observations Beneath Dotson Ice
 671 Shelf, West Antarctica. In Ocean sciences meeting abstracts. Retrieved from
 672 <https://agu.confex.com/agu/osm20/meetingapp.cgi/Paper/653697>
- 673 Errico, R. M. (1997). What is an adjoint model? BAMS, **78**, 2577–2591.
- 674 Gerringa, L. J., Alderkamp, A.-C., Laan, P., Thur'oczy, C.-E., Baar, H. J. D., Mills,
 675 M. M., ... Arrigo, K. R. (2012). Iron from melting glaciers fuels the phytoplank-
 676 ton blooms in amundsen sea (southern ocean): Iron biogeochemistry. Deep Sea
 677 Research Part II: Topical Studies in Oceanography, **71-76**, 16 - 31. Retrieved from
 678 <http://www.sciencedirect.com/science/article/pii/S0967064512000446>
 679 (Shedding Dynamic Light on Fe limitation (DynaLiFe)) doi: [https://doi.org/
 680 10.1016/j.dsr2.2012.03.007](https://doi.org/10.1016/j.dsr2.2012.03.007)
- 681 Giering, R., Kaminski, T., & Slawig, T. (2005, October). Generating efficient deriva-
 682 tive code with TAF adjoint and tangent linear euler flow around an airfoil. Future
 683 Gener. Comput. Syst., **21**(8), 1345–1355. Retrieved from [http://dx.doi.org/10
 684 .1016/j.future.2004.11.003](http://dx.doi.org/10.1016/j.future.2004.11.003) doi: 10.1016/j.future.2004.11.003
- 685 Giles, M. B., Corliss, G., Faure, C., Griewank, A., Hascoët, L., & Naumann,
 686 U. (2002). On the iterative solution of adjoint equations. In Automatic
 687 differentiation of algorithms: From simulation to optimization (pp. 145–151).
 688 New York, NY: Springer New York. Retrieved from [https://doi.org/10.1007/
 689 978-1-4613-0075-5_16](https://doi.org/10.1007/978-1-4613-0075-5_16) doi: 10.1007/978-1-4613-0075-5_16
- 690 Gille, S. T., Metzger, E. J., & Tokmakian, R. (2004, March). Seafloor topography
 691 and ocean circulation. Oceanography, **17**. Retrieved from [https://doi.org/10
 692 .5670/oceanog.2004.66](https://doi.org/10.5670/oceanog.2004.66)
- 693 Goldberg, D. N., Gourmelen, N., Kimura, S., Millan, R., & Snow, K. (2019). How
 694 accurately should we model ice shelf melt rates? Geophysical Research Letters,
 695 **46**(1), 189-199. Retrieved from [https://agupubs.onlinelibrary.wiley.com/
 696 doi/abs/10.1029/2018GL080383](https://agupubs.onlinelibrary.wiley.com/doi/abs/10.1029/2018GL080383) doi: 10.1029/2018GL080383
- 697 Goldberg, D. N., & Heimbach, P. (2013). Parameter and state estimation with a
 698 time-dependent adjoint marine ice sheet model. The Cryosphere, **7**(6), 1659–1678.

- 699 Retrieved from <http://www.the-cryosphere.net/7/1659/2013/> doi: 10.5194/tc
700 -7-1659-2013
- 701 Goldberg, D. N., Heimbach, P., Joughin, I., & Smith, B. (2015). Committed
702 retreat of smith, pope, and kohler glaciers over the next 30 years inferred by
703 transient model calibration. *The Cryosphere*, *9*(6), 2429–2446. Retrieved from
704 <https://www.the-cryosphere.net/9/2429/2015/> doi: 10.5194/tc-9-2429-2015
- 705 Gourmelen, N., N., G. D., Kate, S., F., H. S., G., B. R., Satoshi, K., . . . Jan, B. W.
706 (2017). Channelized melting drives thinning under a rapidly melting antarctic
707 ice shelf. *Geophysical Research Letters*, *44*(19), 9796–9804. Retrieved from
708 <https://agupubs.onlinelibrary.wiley.com/doi/abs/10.1002/2017GL074929>
709 doi: 10.1002/2017GL074929
- 710 Graham, J. A., Dinniman, M. S., & Klinck, J. M. (2016). Impact of model
711 resolution for on-shelf heat transport along the west antarctic peninsula.
712 *Journal of Geophysical Research: Oceans*, *121*(10), 7880–7897. Retrieved from
713 <https://agupubs.onlinelibrary.wiley.com/doi/abs/10.1002/2016JC011875>
714 doi: 10.1002/2016JC011875
- 715 Greene, C. A., Blankenship, D. D., Gwyther, D. E., Silvano, A., & van Wijk, E.
716 (2017). Wind causes totten ice shelf melt and acceleration. *Science Advances*,
717 *3*(11). Retrieved from [https://advances.sciencemag.org/content/3/11/](https://advances.sciencemag.org/content/3/11/e1701681)
718 [e1701681](https://advances.sciencemag.org/content/3/11/e1701681) doi: 10.1126/sciadv.1701681
- 719 Griewank, A., & Walther, A. (2000, March). Algorithm 799: Revolve: An im-
720 plementation of checkpointing for the reverse or adjoint mode of computa-
721 tional differentiation. *ACM Trans. Math. Softw.*, *26*(1), 19–45. Retrieved from
722 <http://doi.acm.org/10.1145/347837.347846> doi: 10.1145/347837.347846
- 723 Griewank, A., & Walther, A. (2008). *Evaluating derivatives. principles*
724 *and techniques of algorithmic differentiation*, vol. 19 of *frontiers in applied*
725 *mathematics* (2nd ed.). Philadelphia: SIAM.
- 726 Gwyther, D. E., Galton-Fenzi, B. K., Hunter, J. R., & Roberts, J. L. (2014). Sim-
727 ulated melt rates for the totten and dalton ice shelves. *Ocean Science*, *10*(3), 267–
728 279. Retrieved from <http://www.ocean-sci.net/10/267/2014/> doi: 10.5194/os
729 -10-267-2014
- 730 Heimbach, P., Hill, C., & Giering, R. (2005). An efficient exact adjoint of the paral-
731 lel MIT general circulation model, generated via automatic differentiation. *Future*

- 732 Generation Computer Systems, 21, 1356–1371.
- 733 Heimbach, P., & Losch, M. (2012). Adjoint sensitivities of sub-ice shelf melt rates to
 734 ocean circulation under Pine Island Ice Shelf, West Antarctica. Annals of Glaciol.,
 735 54, 59–69. doi: 10.3189/2012/AoG60A025
- 736 Heimbach, P., Wunsch, C., Ponte, R. M., Forget, G., Hill, C., & Utke, J. (2011).
 737 Timescales and regions of the sensitivity of atlantic meridional volume and
 738 heat transport: Toward observing system design. Deep Sea Research Part
 739 II: Topical Studies in Oceanography, 58(17), 1858 - 1879. Retrieved from
 740 <http://www.sciencedirect.com/science/article/pii/S0967064511000488>
 741 (Climate and the Atlantic Meridional Overturning Circulation) doi: [https://](https://doi.org/10.1016/j.dsr2.2010.10.065)
 742 doi.org/10.1016/j.dsr2.2010.10.065
- 743 Hellmer, H. H., Kauker, F., Timmermann, R., Determann, J., & Rae, J. (2012).
 744 Twenty-first-century warming of a large antarctic ice-shelf cavity by a redirected
 745 coastal current. Nature, 485(7397), 225-228. Retrieved from [https://doi.org/](https://doi.org/10.1038/nature11064)
 746 [10.1038/nature11064](https://doi.org/10.1038/nature11064) doi: 10.1038/nature11064
- 747 Holland, D. M., Hunter, J., Grosfeld, K., Hellmer, H., Jenkins, A., Morales
 748 Maqueda, M. A., ... Dinniman, M. (2003, December). The Ice Shelf - Ocean
 749 Model Intercomparison Project (ISOMIP). AGU Fall Meeting Abstracts, C41A-
 750 05.
- 751 Holland, D. M., Jacobs, S. S., & Jenkins, A. (2003). Modelling the ocean circulation
 752 beneath the Ross Ice Shelf. Antarctic Science, 15, 13–23.
- 753 Holland, D. M., & Jenkins, A. (1999). Modelling thermodynamic ice-ocean interac-
 754 tions at the base of an ice shelf. J. Phys. Ocean., 29, 1787–1800. doi: [https://doi](https://doi.org/10.1175/1520-0485(1999)029)
 755 [.org/10.1175/1520-0485\(1999\)029](https://doi.org/10.1175/1520-0485(1999)029)
- 756 Hoteit, I., Cornuelle, B., Köhl, A., & Stammer, D. (2005). Treating strong adjoint
 757 sensitivities in tropical eddy-permitting variational data assimilation. Quarterly
 758 Journal of the Royal Meteorological Society, 131(613), 3659–3682. Retrieved
 759 2019-10-21, from [https://rmets.onlinelibrary.wiley.com/doi/abs/10.1256/](https://rmets.onlinelibrary.wiley.com/doi/abs/10.1256/qj.05.97)
 760 [qj.05.97](https://doi.org/10.1256/qj.05.97) doi: 10.1256/qj.05.97
- 761 Hughes, C. W., & Killworth, P. D. (1995). Effects of bottom topography in the
 762 large-scale circulation of the southern ocean. Journal of Physical Oceanography,
 763 25(11), 2485-2497. Retrieved from [https://doi.org/10.1175/1520-0485\(1995\)](https://doi.org/10.1175/1520-0485(1995)025<2485:EOBTIT>2.0.CO;2)
 764 [025<2485:EOBTIT>2.0.CO;2](https://doi.org/10.1175/1520-0485(1995)025<2485:EOBTIT>2.0.CO;2) doi: 10.1175/1520-0485(1995)025<2485:EOBTIT>2.0

765 .CO;2

- 766 Huppert, H. E., & Bryan, K. (1976). Topographically generated eddies. Deep
 767 Sea Research and Oceanographic Abstracts, 23(8), 655 - 679. Retrieved from
 768 <http://www.sciencedirect.com/science/article/pii/S0011747176800137>
 769 doi: [https://doi.org/10.1016/S0011-7471\(76\)80013-7](https://doi.org/10.1016/S0011-7471(76)80013-7)
- 770 Jacobs, S. S., Hellmer, H., & Jenkins, A. (1996). Antarctic ice sheet melting in the
 771 Southeast Pacific. Geophys. Res. Lett., 23, 957–960. doi: [https://doi.org/10.1175/](https://doi.org/10.1175/1520-0485(1999)029)
 772 [1520-0485\(1999\)029](https://doi.org/10.1175/1520-0485(1999)029)
- 773 Jacobs, S. S., Jenkins, A., Giulivi, C., & Dutrieux, P. (2011). Stronger ocean circu-
 774 lation and increased melting under Pine Island Glacier ice shelf. Nat. Geosci. doi:
 775 [10.1038/NGEO1188](https://doi.org/10.1038/NGEO1188)
- 776 Jenkins, A. (2016). A simple model of the ice shelf-ocean boundary layer and
 777 current. Journal of Physical Oceanography, 46(6), 1785-1803. Retrieved from
 778 <http://dx.doi.org/10.1175/JPO-D-15-0194.1> doi: [10.1175/JPO-D-15-0194.1](https://doi.org/10.1175/JPO-D-15-0194.1)
- 779 Jenkins, A., Dutrieux, P., Jacobs, S., Steig, E. J., Gudmundsson, H., Smith, J.,
 780 & Heywood, K. (2016, December). Decadal ocean forcing and antarctic ice
 781 sheet response: Lessons from the amundsen sea. Oceanography, 29. doi:
 782 <https://doi.org/10.5670/oceanog.2016.103>
- 783 Jenkins, A., Dutrieux, P., Jacobs, S. S., McPhail, S. D., Perrett, J. R., Webb, A. T.,
 784 & White, D. (2010). Observations beneath Pine Island Glacier in West Antarctica
 785 and implications for its retreat. Nat. Geosci., 3, 468–472.
- 786 Jenkins, A., & Holland, D. M. (2007). Melting of floating ice and sea level rise.
 787 Geophys. Res. Lett., 34, L16609.
- 788 Jenkins, A., Shoosmith, D., Dutrieux, P., Jacobs, S., Kim, T. W., Le, S. H., ...
 789 Stammerjohn, S. (2018). West antarctic ice sheet retreat in the amundsen
 790 sea driven by decadal oceanic variability. Nat. Geoscience, 11, 733–738. doi:
 791 <https://doi.org/10.1038/s41561-018-0207-4DO>
- 792 Jenkins, A., Vaughan, D. G., Jacobs, S. S., Hellmer, H. H., & Keys, J. R. (1997).
 793 Glaciological and oceanographic evidence of high melt rates beneath Pine Island
 794 Glacier, West Antarctica. Journal of Glaciology, 43(143), 114–121.
- 795 Joughin, I., Smith, B. E., & Medley, B. (2014). Marine ice sheet collapse potentially
 796 under way for the Thwaites Glacier Basin, West Antarctica. Science, 344(6185),
 797 735-738. Retrieved from <http://www.sciencemag.org/content/344/6185/735>

- 798 .abstract doi: 10.1126/science.1249055
- 799 Kimura, S., Adrian, J., Heather, R., R., H. P., M., A. K., B., W. D., ... Pierre,
800 D. (2017). Oceanographic controls on the variability of ice-shelf basal melting
801 and circulation of glacial meltwater in the amundsen sea embayment, antarctica.
802 Journal of Geophysical Research: Oceans, 122(12), 10131-10155. Retrieved from
803 <https://agupubs.onlinelibrary.wiley.com/doi/abs/10.1002/2017JC012926>
804 doi: 10.1002/2017JC012926
- 805 Lilien, D. A., Joughin, I., Smith, B., & Shean, D. E. (2018). Changes in flow of
806 crosson and dotson ice shelves, west antarctica, in response to elevated melt. The
807 Cryosphere, 12(4), 1415–1431. Retrieved from [https://www.the-cryosphere](https://www.the-cryosphere.net/12/1415/2018/)
808 [.net/12/1415/2018/](https://www.the-cryosphere.net/12/1415/2018/) doi: 10.5194/tc-12-1415-2018
- 809 Loose, N., Heimbach, P., Pillar, H., & Nisancioglu, K. (2020). Quantifying Dy-
810 namical Proxy Potential through Oceanic Teleconnections in the North At-
811 lantic. Earth and Space Science Open Archive. Retrieved 2020-03-23, from
812 <https://www.essoar.org/doi/10.1002/essoar.10502065.1> (Publisher: Earth
813 and Space Science Open Archive) doi: 10.1002/essoar.10502065.1
- 814 Losch, M. (2008). Modeling ice shelf cavities in a z coordinate ocean general
815 circulation model. Journal of Geophysical Research: Oceans, 113(C8), n/a–
816 n/a. Retrieved from <http://dx.doi.org/10.1029/2007JC004368> doi:
817 10.1029/2007JC004368
- 818 Losch, M., & Heimbach, P. (2007). Adjoint sensitivity of an ocean general cir-
819 culation model to bottom topography. Journal of Physical Oceanography,
820 37(2), 377-393. Retrieved from <https://doi.org/10.1175/JPO3017.1> doi:
821 10.1175/JPO3017.1
- 822 Marshall, D. (1995). Influence of topography on the large-scale ocean circulation.
823 Journal of Physical Oceanography, 25(7), 1622-1635. Retrieved from [https://doi](https://doi.org/10.1175/1520-0485(1995)025<1622:IOTOTL>2.0.CO;2)
824 [.org/10.1175/1520-0485\(1995\)025<1622:IOTOTL>2.0.CO;2](https://doi.org/10.1175/1520-0485(1995)025<1622:IOTOTL>2.0.CO;2) doi: 10.1175/1520
825 -0485(1995)025<1622:IOTOTL>2.0.CO;2
- 826 Marshall, J., Hill, C., Perelman, L., & Adcroft, A. (1997). Hydrostatic, quasi-
827 hydrostatic, and nonhydrostatic ocean modeling. Journal of Geophysical Research:
828 Oceans, 102(C3), 5733–5752. Retrieved from [http://dx.doi.org/10.1029/](http://dx.doi.org/10.1029/96JC02776)
829 [96JC02776](http://dx.doi.org/10.1029/96JC02776) doi: 10.1029/96JC02776
- 830 Mathiot, P., Jenkins, A., Harris, C., & Madec, G. (2017). Explicit represen-

- 831 tation and parametrised impacts of under ice shelf seas in the z^* coordinate
 832 ocean model nemo 3.6. Geoscientific Model Development, 10(7), 2849–2874.
 833 Retrieved from <https://www.geosci-model-dev.net/10/2849/2017/> doi:
 834 10.5194/gmd-10-2849-2017
- 835 Miles, T., Lee, S. H., Wåhlin, A., Ha, H. K., Kim, T. W., Assmann, K. M., &
 836 Schofield, O. (2016). Glider observations of the Dotson Ice Shelf outflow. Deep Sea
 837 Research Part II: Topical Studies in Oceanography, 123, 16 - 29. Retrieved from
 838 <http://www.sciencedirect.com/science/article/pii/S096706451500301X>
 839 doi: <https://doi.org/10.1016/j.dsr2.2015.08.008>
- 840 Millan, R., Rignot, E., Bernier, V., Morlighem, M., & Dutrieux, P. (2017).
 841 Bathymetry of the Amundsen Sea Embayment sector of West Antarctica from
 842 Operation IceBridge gravity and other data. Geophysical Research Letters, 44(3),
 843 1360-1368. doi: 10.1002/2016GL072071
- 844 Morlighem, M., Rignot, E., Binder, T., Blankenship, D., Drews, R., & others,
 845 . (2020). Deep glacial troughs and stabilizing ridges unveiled beneath the
 846 margins of the antarctic ice sheet. Nature Geoscience, 13(2), 132–137. doi:
 847 10.1038/s41561-019-0510-8
- 848 Nitsche, F. O., Jacobs, S. S., Larter, R. D., & Gohl, K. (2007). Bathymetry of
 849 the amundsen sea continental shelf: Implications for geology, oceanography,
 850 and glaciology. Geochemistry, Geophysics, Geosystems, 8(10). Retrieved from
 851 <https://agupubs.onlinelibrary.wiley.com/doi/abs/10.1029/2007GC001694>
 852 doi: 10.1029/2007GC001694
- 853 Padman, L., Costa, D. P., Bolmer, S. T., Goebel, M. E., Huckstadt, L. A., Jenkins,
 854 A., ... Shoosmith, D. R. (2010). Seals map bathymetry of the antarctic continen-
 855 tal shelf. Geophysical Research Letters, 37(21). doi: 10.1029/2010GL044921
- 856 Petty, A. A., Feltham, D. L., & Holland, P. R. (2013). Impact of Atmospheric
 857 Forcing on Antarctic Continental Shelf Water Masses. Journal of Physical
 858 Oceanography, 43(5), 920-940. Retrieved from [https://doi.org/10.1175/](https://doi.org/10.1175/JPO-D-12-0172.1)
 859 <https://doi.org/10.1175/JPO-D-12-0172.1> doi: 10.1175/JPO-D-12-0172.1
- 860 Pillar, H. R., Heimbach, P., Johnson, H. L., & Marshall, D. P. (2016, Febru-
 861 ary). Dynamical Attribution of Recent Variability in Atlantic Overturn-
 862 ing. Journal of Climate, 29(9), 3339–3352. Retrieved 2019-09-04, from
 863 <https://journals.ametsoc.org/doi/full/10.1175/JCLI-D-15-0727.1> doi:

864 10.1175/JCLI-D-15-0727.1

865 Pritchard, H. D., Ligtenberg, S. R. M., Fricker, H. A., Vaughan, D. G., van den
866 Broeke, M. R., & Padman, L. (2012, April). Antarctic ice-sheet loss driven by
867 basal melting of ice shelves. *Nature*, *484*(7395), 502–505.

868 Randall-Goodwin, E., Meredith, M. P., Jenkins, A., Yager, P. L., Sherrell, R. M.,
869 Abrahamsen, E. P., ... Stammerjohn, S. E. (2015). Freshwater distributions and
870 water mass structure in the Amundsen Sea Polynya region, Antarctica. *Elementa*,
871 *5*, 65. doi: <http://doi.org/10.12952/journal.elementa.000065>

872 Rignot, E., Jacobs, S., Mouginot, J., & Scheuchl, B. (2013). Ice-Shelf Melting
873 Around Antarctica. *Science*, *341*(6143), 266–270. Retrieved from [http://science](http://science.sciencemag.org/content/341/6143/266)
874 [.sciencemag.org/content/341/6143/266](http://science.sciencemag.org/content/341/6143/266) doi: 10.1126/science.1235798

875 Roberts, M. J., & Wood, R. A. (1997). Topographic sensitivity studies with a
876 bryan-cox-type ocean model. *Journal of Physical Oceanography*, *27*(5), 823-
877 836. Retrieved from [https://doi.org/10.1175/1520-0485\(1997\)027<0823:](https://doi.org/10.1175/1520-0485(1997)027<0823:TSSWAB>2.0.CO;2)
878 [TSSWAB>2.0.CO;2](https://doi.org/10.1175/1520-0485(1997)027<0823:TSSWAB>2.0.CO;2) doi: 10.1175/1520-0485(1997)027<0823:TSSWAB>2.0.CO;2

879 Rosier, S. H. R., Hofstede, C., Brisbourne, A. M., Hattermann, T., Nicholls, K. W.,
880 Davis, P. E. D., ... Corr, H. F. J. (2018). A new bathymetry for the southeast-
881 ern filchner-ronne ice shelf: Implications for modern oceanographic processes and
882 glacial history. *Journal of Geophysical Research: Oceans*, *123*(7), 4610-4623. doi:
883 10.1029/2018JC013982

884 Schodlok, M. P., Menemenlis, D., Rignot, E., & Studinger, M. (2012). Sensitivity
885 of the ice-shelf/ocean system to the sub-ice-shelf cavity shape measured by NASA
886 IceBridge in Pine Island Glacier, West Antarctica. *Annals of Glaciology*, *53*(60),
887 156–162.

888 Schoof, C. (2007). Marine ice sheet dynamics. Part I. The case of rapid sliding. *J.*
889 *Fluid Mech.*, *573*, 27–55.

890 Shepherd, A., Wingham, D. J., & Rignot, E. (2004). Warm ocean is eroding West
891 Antarctic Ice Sheet. *Geophys. Res. Lett.*, *31*, L23402.

892 Sirkes, Z., & Tziperman, E. (1997). Finite difference of adjoint or adjoint of fi-
893 nite difference? *Monthly Weather Review*, *125*(12), 3373-3378. Retrieved from
894 [https://doi.org/10.1175/1520-0493\(1997\)125<3373:FDOAOA>2.0.CO;2](https://doi.org/10.1175/1520-0493(1997)125<3373:FDOAOA>2.0.CO;2) doi:
895 10.1175/1520-0493(1997)125(3373:FDOAOA)2.0.CO;2

896 Slater, D. A., Felikson, D., Straneo, F., Goelzer, H., Little, C. M., Morlighem, M.,

- 897 ... Nowicki, S. (2019). 21st century ocean forcing of the greenland ice sheet for
 898 modeling of sea level contribution. The Cryosphere Discussions, 2019, 1–34. Re-
 899 trieved from <https://www.the-cryosphere-discuss.net/tc-2019-222/> doi:
 900 10.5194/tc-2019-222
- 901 Smith, T., & Heimbach, P. (2019). Atmospheric Origins of Variability in the South
 902 Atlantic Meridional Overturning Circulation. Journal of Climate, 32(5), 1483–
 903 1500. Retrieved 2019-02-07, from [http://journals.ametsoc.org/doi/10.1175/](http://journals.ametsoc.org/doi/10.1175/JCLI-D-18-0311.1)
 904 [JCLI-D-18-0311.1](http://journals.ametsoc.org/doi/10.1175/JCLI-D-18-0311.1) doi: 10.1175/JCLI-D-18-0311.1
- 905 Thoma, M., Jenkins, A., Holland, D. M., & Jacobs, S. S. (2008). Modelling Circum-
 906 polar Deep Water intrusions on the Amundsen Sea continental shelf, Antarctica.
 907 Geophys. Res. Lett., 35. doi: 10.1029/2008GL034939
- 908 Thomas, R. H. (1979). The dynamics of marine ice sheets. Journal of Glaciology, 24,
 909 167–177.
- 910 Thomas, R. H., & Bentley, C. R. (1978). A model for the Holocene retreat of the
 911 West Antarctic Ice Sheet. Quaternary Research, 10, 150–170.
- 912 Thompson, A. F., Stewart, A. L., Spence, P., & Heywood, K. J. (2018, December).
 913 The Antarctic Slope Current in a Changing Climate. Reviews of Geophysics,
 914 56(4), 741–770.
- 915 Tinto, K. J., & Bell, R. E. (2011). Progressive unpinning of thwaites glacier
 916 from newly identified offshore ridge: Constraints from aerogravity. Geophysical
 917 Research Letters, 38(20), L20503. Retrieved from [http://dx.doi.org/10.1029/](http://dx.doi.org/10.1029/2011GL049026)
 918 [2011GL049026](http://dx.doi.org/10.1029/2011GL049026) doi: 10.1029/2011GL049026
- 919 Utke, J., Naumann, U., Fagan, M., Tallent, N., Strout, M., Heimbach, P., ... Wun-
 920 sch, C. (2008). OpenAD/F: A modular open source tool for automatic differentia-
 921 tion of Fortran codes. ACM Transactions on Mathematical Software, 34.
- 922 Wählin, A. K., Steiger, N., Darelius, E., Assmann, K. M., Glessmer, M. S., Ha,
 923 H. K., ... Viboud, S. (2020, February). Ice front blocking of ocean heat trans-
 924 port to an Antarctic ice shelf. Nature, 578(7796), 568–571. Retrieved 2020-02-28,
 925 from <http://www.nature.com/articles/s41586-020-2014-5> (Number: 7796
 926 Publisher: Nature Publishing Group) doi: 10.1038/s41586-020-2014-5
- 927 Walker, D. P., Jenkins, A., Assmann, K., Shoosmith, D., & Brandon, M. (2013).
 928 Oceanographic observations at the shelf break of the Amundsen Sea, Antarctica.
 929 Journal of Geophysical Research: Oceans, 118(6), 2906-2918. Retrieved from

- 930 <https://agupubs.onlinelibrary.wiley.com/doi/abs/10.1002/jgrc.20212>
931 doi: 10.1002/jgrc.20212
- 932 Webber, B., Heywood, K., Stevens, D. P., Dutrieux, P., Abrahamsen, E. P., Jenk-
933 ins, A., ... Kim, T. W. (2017, February). Mechanisms driving variability in the
934 ocean forcing of Pine Island Glacier. *Nature Communications*, *8*, 14507. doi:
935 10.1038/ncomms14507
- 936 Wei, W., Blankenship, D. D., Greenbaum, J. S., Gourmelen, N., Dow, C. F., Richter,
937 T. G., ... Assmann, K. M. (2019). Getz ice shelf melt enhanced by freshwater
938 discharge from beneath the west antarctic ice sheet. *The Cryosphere Discussions*,
939 *2019*, 1–16. Retrieved from [https://www.the-cryosphere-discuss.net/
940 tc-2019-170/](https://www.the-cryosphere-discuss.net/tc-2019-170/) doi: 10.5194/tc-2019-170
- 941 Wunsch, C. (1996). *The ocean circulation inverse problem*. New York: Cambridge
942 University Press.
- 943 Wunsch, C., & Heimbach, P. (2007). Practical global ocean state estimation.
944 *Physica D*, *230*, 197–208.
- 945 Wunsch, C., Ponte, R., Heimbach, P., & Fukumori, I. (2009). The global general
946 circulation of the ocean estimated by the ecco-consortium. *Oceanography*, *22*, 88-
947 103.
- 948 Yager, P. L., Sherrell, R. M., Stammerjohn, S. E., Alderkamp, A.-C., Schofield, O.,
949 Abrahamsen, E. P., ... Wilson, S. (2012, September). Aspire: The amundsen sea
950 polynya international research expedition. *Oceanography*, *25*. Retrieved from
951 <https://doi.org/10.5670/oceanog.2012.73>
- 952 Zhang, X., Thompson, A. F., Flexas, M. M., Roquet, F., & Bornemann, H.
953 (2016). Circulation and meltwater distribution in the bellingshausen sea: From
954 shelf break to coast. *Geophysical Research Letters*, *43*(12), 6402-6409. doi:
955 10.1002/2016GL068998
- 956 Zhao, K. X., Stewart, A. L., & McWilliams, J. C. (2018, November). Sill-Influenced
957 Exchange Flows in Ice Shelf Cavities. *Journal of Physical Oceanography*, *49*(1),
958 163–191. Retrieved 2019-06-05, from [https://journals.ametsoc.org/doi/full/
959 10.1175/JPO-D-18-0076.1](https://journals.ametsoc.org/doi/full/10.1175/JPO-D-18-0076.1) doi: 10.1175/JPO-D-18-0076.1

960

961

The submitted manuscript has been created by UChicago Argonne, LLC, Operator of Argonne National Laboratory ('Argonne'). Argonne, a U.S. Department of Energy Office of Science laboratory, is operated under Contract No. DE-AC02-06CH11357. The U.S. Government retains for itself, and others acting on its behalf, a paid-up nonexclusive, irrevocable worldwide license in said article to reproduce, prepare derivative works, distribute copies to the public, and perform publicly and display publicly, by or on behalf of the Government. The Department of Energy will provide public access to these results of federally sponsored research in accordance with the DOE Public Access Plan. <http://energy.gov/downloads/doe-public-access-plan>.

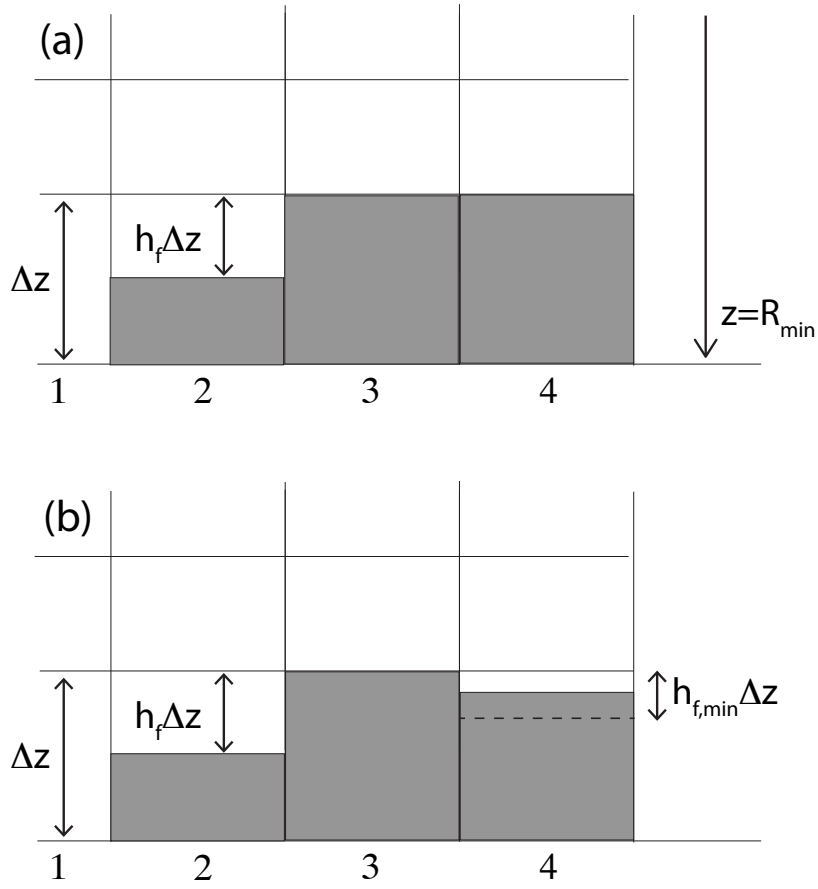


Figure 1. (a) A schematic (adapted from <http://mitgcm.org/>) of the representation of bottom topography in MITgcm. The white regions within cells contain fluid. In column 1, all cells are fluid-filled and the bathymetry is R_{\min} . The bottom cells of Columns 3 and 4 are non-fluid-containing, and in these columns the bottom elevation is $R_{\min} + \Delta z$. In Column 2, the bottom cell is a partial cell, and bathymetry is $R_{\min} + (1 - h_f)\Delta z$. The interface between the bottom cells of Column 1 and Column 2 has height $h_f \Delta z$, and there is no interface between the bottom cell of Column 2 with any cell in Column 3. (b) A perturbation to bathymetry is made, indicated by gray shading in to bottom cell of Column 4. Depending on the size of the perturbation, ocean model initialisation may lower bathymetry further so that the liquid-containing portion of the bottom cell is $h_{f,\min} \Delta z$; or it may restore bathymetry to that of (a).

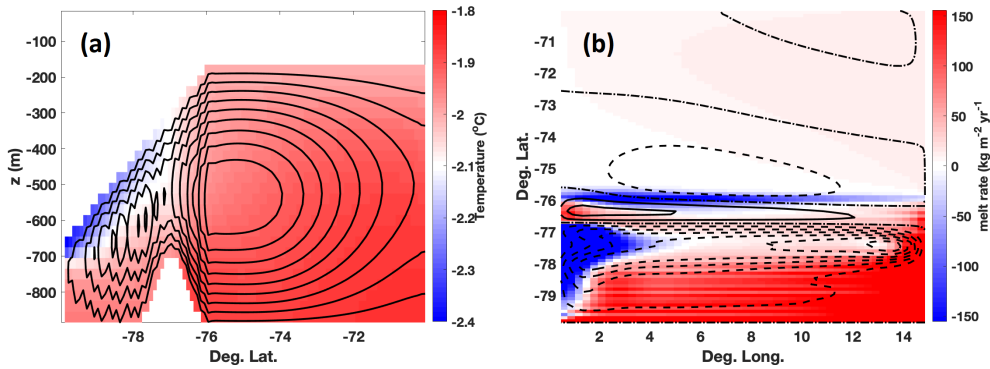


Figure 2. (left) Zonally averaged temperature (shading) and overturning stream function (contours) in the modified ISOMIP experiment. The profile of the “ridge” is apparent between -78° and -76° Latitude. (right) Melt rate at the termination of the experiment (shading; negative values indicate accretion) and depth-integrated stream function (contours; dashed lines where negative).

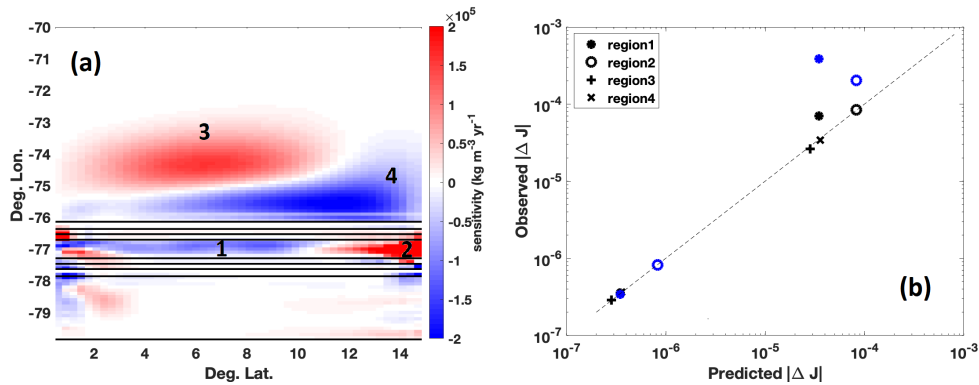


Figure 3. (left) Domain bathymetry (contours; 50m isolines) and sensitivity of spatially-integrated melt at model termination to bathymetry (shading); value of sensitivity in a cell indicates gradient of melt with respect to elevation in the cell, where positive (negative) values indicate regions where raising (lowering) the bottom will increase melt. (right) Comparison of perturbed objective function (in Gt/a melt) with value predicted by linearized sensitivities, as described in Section 3.1. Blue markers indicate negative perturbations while black markers indicate positive ones. Small values (less than 10^{-6} Gt/a) indicate perturbations scaled by 0.1m and large values (greater than 10^{-5} Gt/a) indicate perturbations scaled by 10m. Though the *sign* of the observed ΔJ is not given, it is in all cases the same as the prediction.

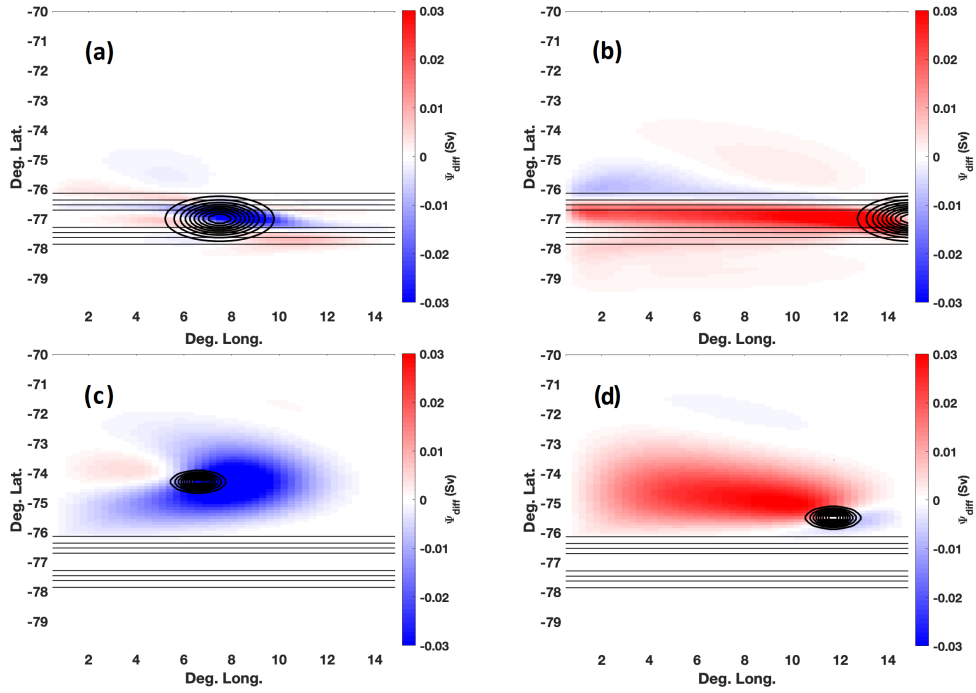


Figure 4. Perturbed beds (thick contours), background bathymetry (thin contours; 50m isolines) and corresponding perturbed stream functions (shading) in different regions of high sensitivity in Fig. 3 (a) through (d) correspond to finite perturbations in locations (1) through (4) in Fig. 3(a), respectively. Bathymetric perturbations plotted with $\delta R=10$ (Eqn. 3) and 1m isolines.

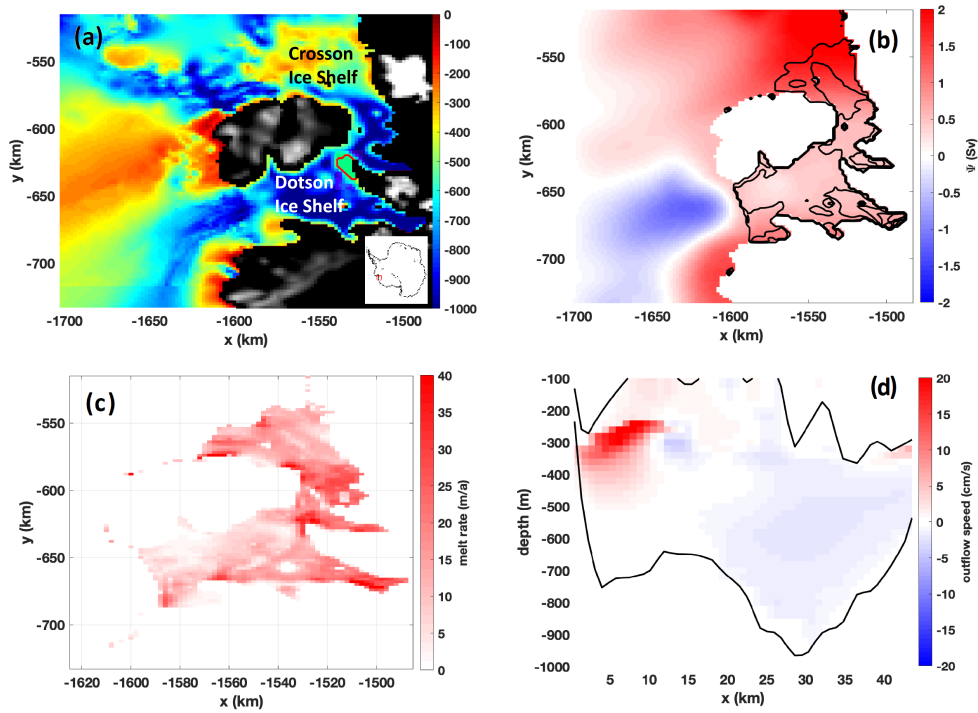


Figure 5. (a) The bathymetry of Millan et al. (2017), used in our adjoint experiment. Black and white shading indicates topography above sea level. X and Y coordinates refer to a Polar Stereographic projection. The red contour near the junction of Dotson and Crosson ice shelves indicates where bathymetry has been modified from Millan et al. (2017) as discussed in Section 4.1. (b) The barotropic stream function corresponding to the initial steady state of the ocean model. (c) Under-ice shelf melt rate corresponding to the steady state. (d) Outflow at the opening to the Dotson Ice Shelf cavity cf. Randall-Goodwin et al. (2015), their Figure 7(a)).

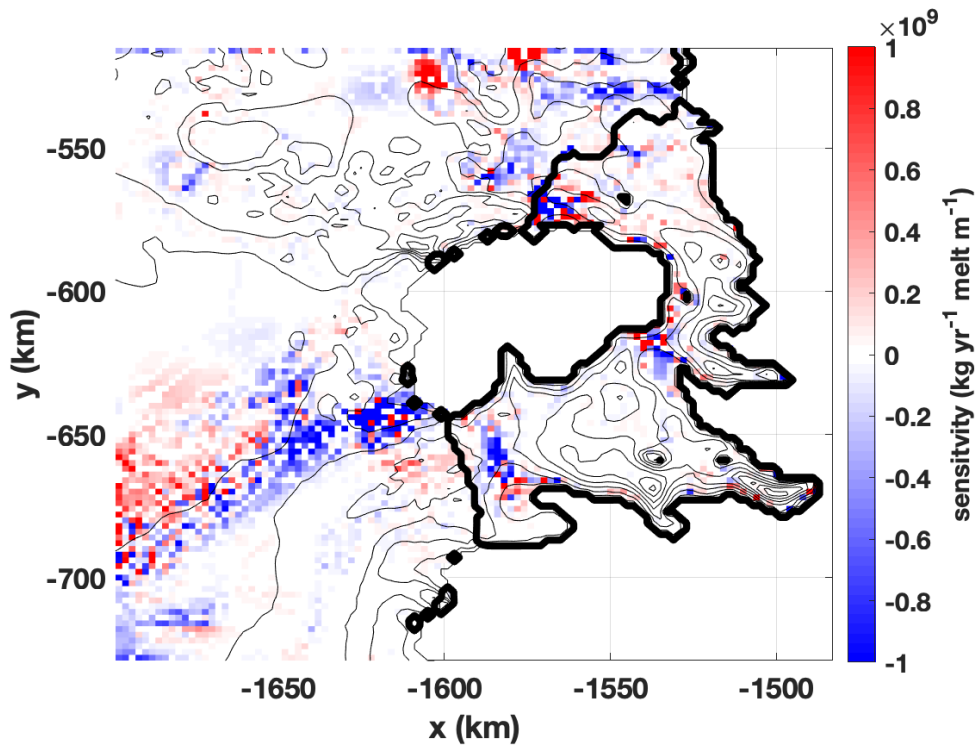


Figure 6. Sensitivity of total (area-integrated) melt to bathymetry in Dotson-Crosson experiment; interpretation is as in Fig. 3(a).

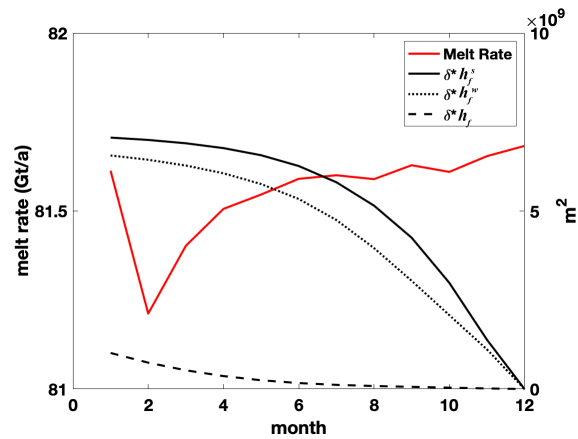


Figure 7. Time series of melt volume and bathymetric sensitivity factors in our simulation of Dotson and Crosson ice shelves. Note sensitivity fields computed from the adjoint model evolve backward in time.

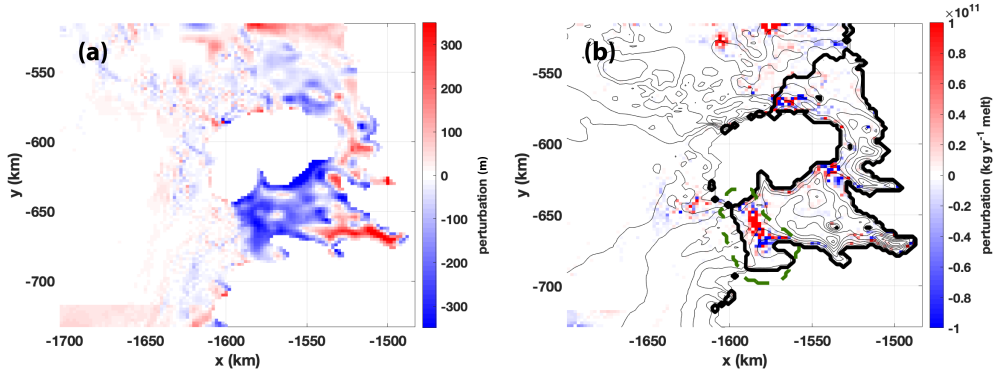


Figure 8. (a) Difference between BedMachine bathymetry and Millan bathymetry within the ocean model domain. The rectangular region in the bottom left of the figure is due to the Millan data set not extending to the edge of the domain. (b) The product of this difference and the sensitivity of melt with respect to bathymetry. The region enclosed by the dashed contour accounts for approximately 4.3 Gt/yr of the linear-predicted melt rate difference.

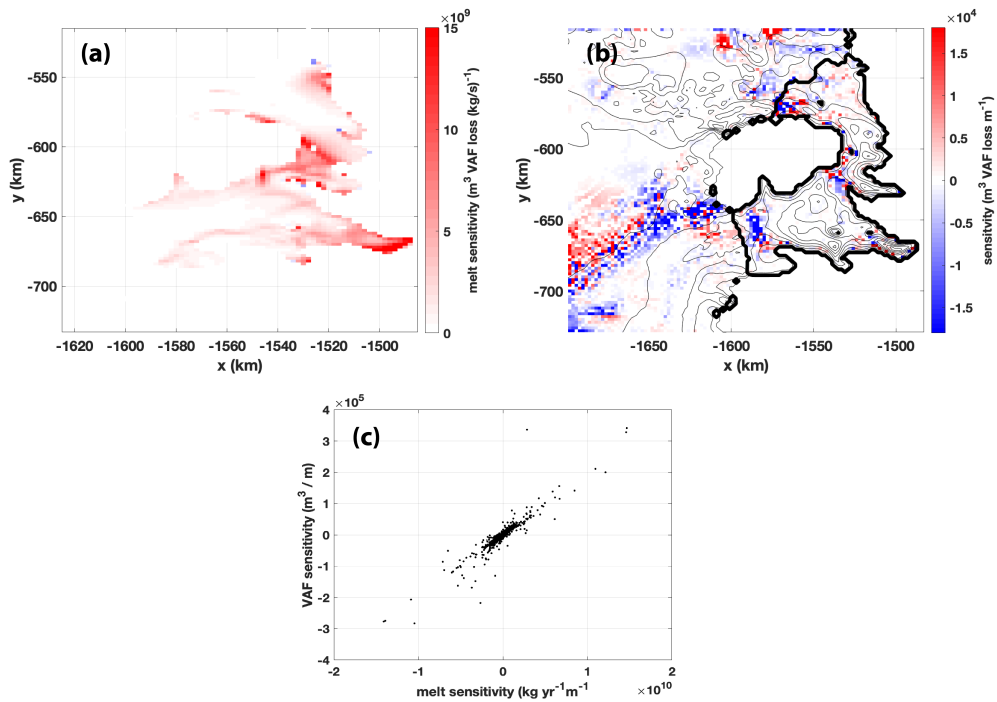


Figure 9. (a) Sensitivity of grounded ice volume to ice-shelf melt (adapted from Goldberg et al. (2019), their Fig. 3(b)). (b) Sensitivity of the objective function given by Eqn. (6) to bathymetry. (c) Cell-by-cell correspondence of grounded volume sensitivity to melt-rate sensitivity.

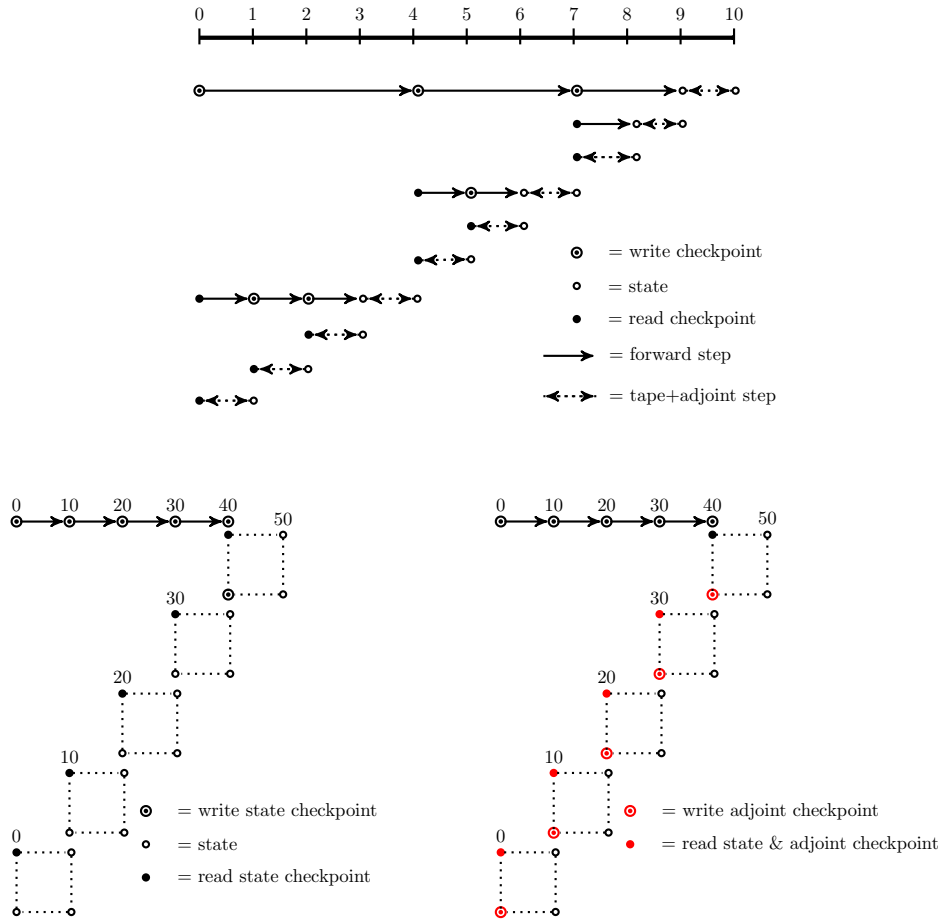


Figure 10. Top: Binomial checkpointing schedule for $l = 10$ time steps and $c = 3$ checkpoints. Bottom Left: Two level checkpointing schedule for $l = 50$ with ($l_2 = 5$) outer level iterations and ($l_1 = 10$) inner level iterations. Periodic checkpointing is used in the outer level and binomial checkpointing shown by the dashed box is used at the inner level. Bottom Right: Enhanced two level checkpointing schedule with support for resilient adjoints through the writing and reading of the adjoint state at the outer level.